DESIGN AND CONSTRUCTION OF A 1 MeV CYCLOTRON

by

Ebru Şimşek

B.S., Physics, Boğaziçi University, 2014

Submitted to the Institute for Graduate Studies in
Science and Engineering in partial fulfillment of
the requirements for the degree of
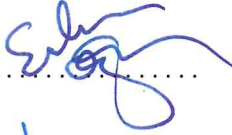Master of Science

Graduate Program in Physics

Boğaziçi University

2019

DESIGN AND CONSTRUCTION OF 1 MeV CYCLOTRON

APPROVED BY:

Prof. Veysi Erkcan Özcan
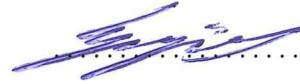(Thesis Supervisor)

Assoc. Prof. Bora Işıldak
(Thesis Co-supervisor)

Assoc. Prof. Alper Hayreter

Prof. Erhan Gülmez

Prof. Mehmet Burçin Ünlü

DATE OF APPROVAL: 24.05.2019

To the memory of successful high-energy physicist Prof. Engin Arık,

ACKNOWLEDGEMENTS

Firstly, I would like to express my sincere gratitude to my advisor Prof. V. Erkcan Özcan for his guidance and endless support throughout my studies. He also deserves special thanks for encouraging me being a physicist.

I would also like to thank to my co-advisor Dr. Bora Işıldak for the continuous support of my thesis study and his patience, motivation, and immense knowledge. His guidance helped me in all the time of research and writing of this thesis.

I am also happy to work with Dr. Alper Hayreter who has dedicated his time and consideration for my studies. I am also grateful for his invaluable support in the laboratory works.

I want to express my thanks to Metal Yapı family for their technical support and guidance. I specially thank Aylin Özgül, Bülent Özgül and Selami Gürel for their support throughout this project. They were very encouraging and sincere.

I specially thank Nur Banu and Murat for their friendship and invaluable support.

Last but not the least, I specially thank my parents Selime and Mehmet Ali Şimşek, my brother Erhan, my sisters Dilek and Filiz for supporting me throughout my years of study and writing this thesis. This journey would not have been possible without them. Thank you.

ABSTRACT

DESIGN AND CONSTRUCTION OF A 1 MeV CYCLOTRON

This thesis studies the design and construction of Turkey's first 1 MeV cyclotron. The iron yoke, electromagnets and vacuum chamber, which are its main components, have been constructed. Electrically insulated electromagnets have been assembled using copper profile pipes at the Özyeğin University Particle Accelerator Laboratory. Applying a direct current to magnet coils, an almost uniform magnetic field has been achieved between the poles. Magnetic field values obtained from the simulations are compatible with measured magnetic values. Furthermore, betatron oscillations have been observed in the ion path simulation computed with the 4th order Runge Kutta method. Near future goals are the connection of a custom-designed RF power amplifier and the measurement of flow parameters which have already been calculated for the cooling system.

ÖZET

1 MeV SİKLOTRON TASARIMI VE YAPIMI

Bu tezde, Türkiye'de ilk kez 1 MeV enerji düzeyinde klasik bir siklotronun tasarım ve yapım aşamaları anlatılmıştır. Siklotronun ana bileşenlerinden olan demir gövde, elektromıknatıslar ve vakum odası tamamlanmıştır. Elektrik yalıtımlı elektromıknatıslar, bakır profil borular kullanılarak Özyeğin Üniversitesi Parçacık Hızlandırıcı Laboratuvarı'nda üretilmiştir. Elektromıknatıslara doğru akım uygulanarak neredeyse homojen bir manyetik alan elde edilmiştir. Simülasyondan elde edilen manyetik kutuplar arasındaki manyetik alan değerleriyle ölçülen manyetik alan değerleri birbiriyle uyumludur. Ayrıca 4. mertebe Runge Kutta yöntemiyle elde edilen iyon yörünge simülasyonunda betatron osilasyonları gözlemlenmiştir. Soğutma sistemi için hesaplanmış olan akış parametrelerinin ölçümü ve özel üretim RF yükseltgecinin tamamlanıp sisteme dahil edilmesi yakın gelecek planlarındandır.

TABLE OF CONTENTS

LIST OF FIGURES

LIST OF TABLES

LIST OF SYMBOLS

Z$_{load}$ Impedance of the Cyclotron

Z$_{source}$ Impedance of the Generator

Γ Reflection Ratio

LIST OF ACRONYMS/ABBREVIATIONS

2D	Two Dimensional
3D	Three Dimensional
A	Amper
AC	Alternating Current
CSV	Comma-separated Values
dBm	Decibel-Milliwatts
DC	Direct Current
FDG	Fluoro Deoxy Glucose
keV	Kilo Electron Volt
kV	Kilo Volt
MV	Mega Volt
MeV	Mega Electron Volt
PSF	Poisson SuperFish
RF	Radio Frequency
Re	Reynolds Number
RK4	Runge Kutta Fourth Order
V_{fwd}	Forward Voltage Signal
V_{ref}	Reflected Voltage Signal
VSWR	Voltage Standing Wave Ratio

1. INTRODUCTION

Democritus, an Ancient Greek philosopher in the fifth century BC, suggested that everything in universe is made up of small, indivisible pieces. He called these small things atoms and defined an atom as the smallest indivisible building block of everything. In the middle of 1800s, John Dalton also advocated the Democritus' idea of atoms. Dalton's atomic model is very similar to that of Democritus'.

In 1897, discovery of electron by J.J.Thomson was a milestone for atomic physics. This discovery showed that there are smaller particles inside an atom; therefore, it can be divided. A few years later, he created the so-called "plum pudding model" of the atom, as he asserted that both negative and positive charges place irregularly in an atom.

Ernest Rutherford carried a step further the idea of charged particles. Rutherford and his colleague Hans Geiger's gold foil experiment changed everything known about atomic structure. They sent positively charged alpha particles to the gold foil. They were expecting that the particles penetrate through the foil and scatter slightly. However, a small number of the alpha particles scattered with a wide angle. They explained the result of the experiment as: "An atom substantially consists of empty space but it has a dense and positively charged region in the center." This phenomenon was clarified by the idea of a nucleus: Rutherford proposed that electrons orbit around a positively charged atomic nucleus and there is empty space between them. Rutherford's atom model was close to today's description of atomic structure.

After the discovery of nucleus, Rutherford started studies about "splitting of the atom". He was thinking that it would be a good method to send high velocity particles towards to nucleus in order to understand the inner structure of an atom. With the latest developments, acceleration of particles became an important subject around 1920. However, particle accelerators would need to be constructed as a first step to speed up the particles.

John Cockroft and Ernest Walton, who were students of Rutherford, decided to make a generator in order to get high DC voltages. Accelerating particles to very high speeds would therefore be possible. Cockcroft-Walton accelerator is an electrostatic particle accelerator, which makes use of many diodes and capacitors (Figure 1.1). Supplied alternating voltage is gradually multiplied with the help of these capacitors and diodes. Cockroft and Walton succeeded accelerating protons up to 400 kV and collided them with the Lithium atom. The Lithium nucleus was split by accelerated protons and separated into two Helium nuclei. However, the limit of Cockroft-Walton generator was around 1.5 MV.
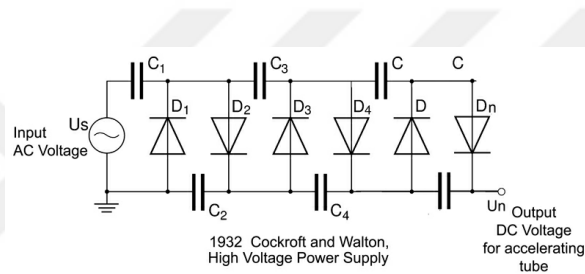
Figure 1.1. Scheme of Cockroft-Walton Generator [1].

Another type of electrostatic accelerator is based on the Van de Graaff Generator (Figure 1.2). The physics behind the Van de Graaff Generator is triboelectricity, which is taught even to children with the plastic strip and woollen cloth experiment. When a plastic strip is rubbed with woolen cloth, they exchange electrons. Likewise, in a Van de Graaff Generator there is a comb and conveyor belt system. The belt is rotated by a motor and comb rubs to belt. As a result, charges accumulate on the surface of metal sphere via collecting comb. More charges mean more potential on the metal sphere. This potential is used for accelerating the ions.
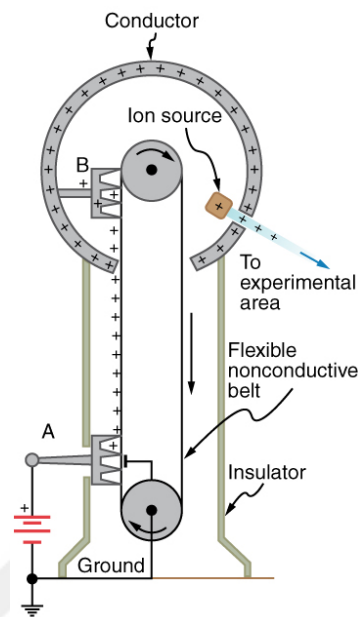
Figure 1.2. A scheme of Van de Graaff Generator [2].

The upper limit of a Van de Graaff Generator is approximately 20 MV because of Corona discharge. When the electric field on the surface of conductor(metal sphere) reaches the breakdown value, charges leak out from sphere to air(or other gas). Therefore, the potential of conductor no more increases [5].

Limited energy scale of electrostatic accelerators was restricting the research on atomic structure. Instead of electrostatic generators, Gustav Ising suggested using alternating current sources to defeat energy restriction. And he created a linear accelerator model composed of successive drift tubes. A graduate student Rolf Wideroe developed Ising's linear accelerator idea. Wideroe designed a linear accelerator that gives energy to ions resonating them with the radio frequency.

Wideroe, was also thinking about using the same voltage many times to accelerate the particles. So, ions could be accelerated without requiring a single very high voltage supply. Using the same voltage for many times could be possible by a cyclic path. Ernest Lawrence put this idea into practice. In 1929, he invented the first circular accelerator, a cyclotron, that accelerates charged particles in a circular trajectory taking advantage of electric and magnetic fields.

Cyclotron is both compact and cost effective in comparison to linear accelerators. If it is intended to reach high energy levels, the length of linear accelerators must be extended. In this respect, cyclotrons advantages over present linear accelerators.

When a cyclotron operates, both electric and magnetic fields are applied on the particles. Therefore, Lorentz force exerts on them (Equation 1.1). Ions are exposed to electric field only between the dees. The dees act as a Faraday cage thus there is no electric field inside them. Therefore, the only force on the particles when they are inside is the magnetic force.

If charged particles with a constant speed are subjected to uniform magnetic field, they move in a circular path. For a cyclotron, radius of trajectory increases in each turn because the particles gain energy via the electric field every time they pass between the dees. So, the ion path becomes spiral-like because the radius of curvature increases with the increasing velocity (Equation 1.2).

$$\vec{F} = q(\vec{E} + \vec{v} \times \vec{B}) \qquad (1.1)$$

$$\frac{mv^2}{r} = qvB \qquad r = \frac{mv}{qB} \qquad (1.2)$$

The crucial point for the operation of a cyclotron is timing of the electric field. Quoting M.S.Livingston: *In the summer of 1930 I asked Prof. Lawrence to propose a topic for an experimental thesis. He suggested a study of the resonance of hydrogen ions with a radio frequency field in the presence of a magnetic field – the phenomenon now known as cyclotron resonance* [6].

To accelerate the particles between the dees, the frequency of RF source must be synchronized with gyro-frequency of ions. $f = \frac{qB}{2\pi m}$ so the frequency of ions depend only on the strength of the magnetic field. Therefore, magnetic field, B, must be uniform to keep the gyro-frequency of ions fixed for increasing radius.

The first cyclotron was constructed by E.Lawrence and M.S.Livingston had a diameter of approximately 4.5 inches, and accelerated hydrogen ions up to 80 keV using a 1.8 keV generator. By January 9, 1932, they had built a larger 1D-inch model, which achieved to produce 1 MeV protons [7].

Until today, many cyclotrons have been built in different energies and sizes. Nowadays, they are generally used for medical purposes especially in the commercial production of F^{18} radioisotope. F^{18} has half life of 1.8 hours, and is produced by proton bombardiment of oxygen-rich water, containing ^{18}O isotope of oxygen. F^{18} combined with deoxy-glucoseto synthesize the commonly used radioactive tracer ^{18}FDG. Since cancer cells consume more energy than that of healthy ones, in case ^{18}FDG is taken by a patient, it is intensely demanded by cancerous tissues. Therefore, large amount of the ^{18}FDG goes to tumor cells. When, F^{18} decays, it emits positrons. When these positrons meet with the electron of surrounding atoms, they annihilate each other. As a result of the annihilation, gamma rays are emitted. Intense gamma radiation reveals the location of the tumors.

There is another important cyclotron-produced radioisotope, Technetium-99m (Tc-99m). Tc-99m was actually discovered in 1938 by Emilio Segre. After a visit to Ernest O. Lawrence's Berkeley Radiation Laboratory, Segre was sent a molybdenum strip from the laboratory's cyclotron deflector in 1937 that was emitting anomalous forms of radioactivity. After careful chemical and theoretical analysis, Segrè was able to prove that some of the radiation was being produced by a previously unknown element, dubbed Technetium [8]. Nowadays, a large majority of it is produced in nuclear reactors. However, aging reactors and the high costs of their maintenance, radioactive waste processing, and final re-actor decommissioning make the use of safe and relatively low-cost cyclotron technology more attractive today for regional supply of Tc-99m [9].

Technetium-99m (Tc-99m) is the most used radionuclide in nuclear medicine imaging. Beside radioisotope productions, cyclotrons are also used for cancer treatments such as radiotherapy and particle therapy.

1.1. Main Components of Cyclotrons

Although design and energy scale show variations according to intended use, all types of cyclotrons have the same general structure. They have 3 fundamental mechanical parts; electromagnets, iron yoke and vacuum chamber. Various components of a cyclotron will be explained later in more detail.

A DC current is applied to coils, so magnetic field is created between the 2 magnetic poles. Magnetic field is not only for keeping the particles in a circular path, but also for focusing the beam.

Solid iron yoke is required for permeating the magnetic field. Iron yoke enables the uniformity of both the direction and magnitude of the magnetic field. Adherence to uniformity is crucial to keep the rotation frequency of the ions constant and hence match the RF system.

| (a) | (b) |

Figure 1.3. A vacuum chamber with 2-Dees [3] and iron yoke of the OZU Cyclotron
in (a), (b) respectively.

Vacuum chamber, located between the magnet poles, houses one or more D shaped electrodes (though in some designs, the dees are no longer D shaped, just circular arcs) and the ion source, vacuum system and several ports. Ion source is located at the center of the machine, in the middle of the electrodes. It can be used to obtain either positive or negative ions. In many commercial applications, ions are generally created by ionizing hydrogen gas (H_2).

When the charged particles are released from the ion source, they are exposed to the electric field between the dees and go toward oppositely charged dee. After completing their semi circular trajectory, they reach again a gap between the dees and they are again accelerated by the electric field. However, this time they are pulled by the other dee because alternating voltage reverses polarity of the dees. This process repeats until the beam is extracted.

While ions are moving in their circular trajectories, it is important that they do not collide with any gas molecules on their ways. Any such collision may lead to energy loss and straying from the orbit. In this respect, the mean free path must be considered. Mean free path is the average distance a particle travels without a collision or the average distance between two consecutive collisions.

$$\lambda = \frac{RT}{\sqrt{2}\pi d^2 N_A P} \tag{1.3}$$

λ: Mean free path

R: Universal gas constant (8.3145 J/mol K)

T: Temperature in Kelvin

d: Diameter of molecule

N_A: Avagadro's number (6.0221×10^{23} mol^{-1})

P: Pressure

As it can be seen from Equation 1.3, lower vacuum pressure means longer mean free path. Therefore, pressure must be as low as possible to avoid interactions with other particles.

2. THEORY

In this chapter, motion of the ions will be analyzed by expressing the Lorentz force in cylindrical coordinates. Therefore, first the cylindrical coordinates are defined below.

$$\hat{r} = \cos\theta\hat{i} + \sin\theta\hat{j}, \quad \hat{\theta} = -\sin\theta\hat{i} + \cos\theta\hat{j}, \quad \hat{z} = \hat{k} \tag{2.1}$$

$$\dot{\hat{r}} = \dot{\theta}\hat{\theta}, \quad \dot{\hat{\theta}} = -\dot{\theta}\hat{r}, \quad \dot{\hat{z}} = 0 \tag{2.2}$$

$$\vec{\rho} = r\hat{r} + z\hat{z} \qquad \vec{v} = r\dot{\hat{r}} + \dot{r}\hat{r} + \dot{z}\hat{z} + z\dot{\hat{z}} \tag{2.3}$$

Then, the equation of motion is constructed using Newton's Second Law.

$$m\vec{a} = q(\vec{E} + \vec{v} \times \vec{B}) \tag{2.4}$$

$$\vec{E} = E_r\hat{r} + E_\theta\hat{\theta} + E_z\hat{z} \qquad \vec{B} = B_r\hat{r} + B_\theta\hat{\theta} + B_z\hat{z} \tag{2.5}$$

$$\vec{a} = \ddot{r}\hat{r} + \dot{r}\dot{\hat{r}} + (\dot{r}\dot{\theta} + r\ddot{\theta})\hat{\theta} + (r\dot{\theta})\dot{\hat{\theta}} + \ddot{z}\hat{z} + \dot{z}\dot{\hat{z}} = (\ddot{r} - r\dot{\theta}^2)\hat{r} + (2\dot{r}\dot{\theta} + r\ddot{\theta})\hat{\theta} + \ddot{z}\hat{z} \tag{2.6}$$

$$\begin{aligned} \vec{v} \times \vec{B} &= (\dot{r}\hat{r} + r\dot{\theta}\hat{\theta} + \dot{z}\hat{z}) \times (B_r\hat{r} + B_\theta\hat{\theta} + B_z\hat{z}) \\ &= \dot{r}B_\theta\hat{z} - \dot{r}B_z\hat{\theta} - r\dot{\theta}B_r\hat{z} + r\dot{\theta}B_z\hat{r} + \dot{z}B_r\hat{\theta} - \dot{z}B_\theta\hat{r} \\ &= (r\dot{\theta}B_z - \dot{z}B_\theta)\hat{r} + (\dot{z}B_r - \dot{r}B_z)\hat{\theta} + (\dot{r}B_\theta - r\dot{\theta}B_r)\hat{z} \end{aligned} \tag{2.7}$$

Combining Equations 2.5, 2.6 and 2.7, equation of motion can be obtained easily:

$$m((\ddot{r} - r\dot{\theta}^2)\hat{r} + (2r\dot{\theta} + r\ddot{\theta}) + \ddot{z}\hat{z})$$
$$= q((E_r + \dot{\theta}B_z - \dot{z}B_\theta)\hat{r}) + (E_\theta + \dot{z}B_r - \dot{r}B_z)\hat{\theta}) + (E_z + \dot{r}B_\theta - r\dot{\theta}B_r)\hat{z})$$

$$(2.8)$$

It will be useful separating the equation of motion into r, θ and z components;

$$m(\ddot{r} - r\dot{\theta}^2) = q(B_z r\dot{\theta} - B_\theta \dot{z}) \tag{2.9}$$

$$m(2\dot{r}\dot{\theta} + 2r\ddot{\theta}) = q(\dot{z}B_r - B_z\dot{r}) \tag{2.10}$$

$$m\ddot{z} = q(\dot{r}B_\theta - r\dot{\theta}B_r) \tag{2.11}$$

Electric field is effective only between the dees. There is no electric field inside the dees. Therefore, ions are only exposed to magnetic field when they are inside the dees.

The axial component of magnetic field, B_z, is almost uniform but it decreases very slowly with an increasing r. These small variations should be taken into consideration in defining B_z. Consequently, B_z İs described using first order Taylor expansion around some equilibrium orbit r_0 with a small deviation x.

$$
\begin{aligned}
B_z(r) &= B_z(r_0) + \frac{\partial B_z}{\partial r}(r - r_0) \\
&= B_z(r_0) + \frac{\partial B_z}{\partial x}x \\
&= B_z(r_0)\left(1 + \frac{x}{B_z(r_0)}\frac{\partial B_z}{\partial x}\right) \\
&= B_z(r_0)\left(1 - \frac{x}{r_0}\left(-\frac{r_0}{B_z(r_0)}\frac{\partial B_z}{\partial x}\right)\right)
\end{aligned} \tag{2.12}
$$

Here, $B_z(r_0)$ represents the axial component of magnetic field at some equilibrium orbit r_0 where $r = r_0 + x$ and $x \ll r_0$. In general, $B_z(r)$ is expressed in terms of field index in Equation 2.13 . Field index was first introduced by D.W.Kerst and R.Serber [10]. As it can be seen from Equation 2.14, $B_z(r)$ can be arranged using the field index.

$$
n = -\frac{r_0}{B_z(r_0)}\frac{\partial B_z}{\partial x} \tag{2.13}
$$

$$
B_z(r) = B_z(r_0)\left(1 - \frac{x}{r_0}n\right) \tag{2.14}
$$

If all particles were exactly on orbit, the equation of motion would be $\frac{mv^2}{r} = qvB_z$. However, ions that are off the orbit experience another restoring force $F_r = \frac{mv^2}{r} - qvB_z$.

$$
F_r = \frac{mv^2}{r} - qvB_z(r_0)\left(1 - \frac{nx}{r_0}\right) \tag{2.15}
$$

$$
\frac{1}{r} = \frac{1}{r_0 + x} = \frac{1}{r_0}\left[\frac{1}{1 + \frac{x}{r_0}}\right] = \frac{1}{r_0}\left[1 + \frac{x}{r_0}\right]^{-1} \approx \frac{1}{r_0}\left[1 - \frac{x}{r_0}\right] \tag{2.16}
$$

$$
F_r = mv^2\frac{1}{r_0}(1 - \frac{x}{r_0}) - qvB_z(r_0)\left(1 - \frac{nx}{r_0}\right) \tag{2.17}
$$

$$F_r = \frac{mv^2}{r_0}\left(1 - \frac{x}{r_0}\right) - \frac{mv^2}{r_0}\left(1 - \frac{nx}{r_0}\right) = \frac{mv^2}{r_0}\frac{x}{r_0}(n-1) \tag{2.18}$$

Equation 2.18 can be simplified using $\frac{v}{r_0} = \omega_0$ where w_0 is gyro frequency.

$$m\ddot{x} + m\omega_0^2(1-n)x = 0 \tag{2.19}$$

Finally, dividing Equation 2.19 by m, it turns into Kerst-Serber equation for horizontal motion [10], see Equation 2.20.

$$\ddot{x} + \omega_0^2(1-n)x = 0 \tag{2.20}$$

Solution of the Kerst-Serber equation is:

$$x = x_{max}\sin(\sqrt{1-n}\,\omega_0 t) \tag{2.21}$$

$$\omega_r = \omega_0\sqrt{1-n} \tag{2.22}$$

$$\frac{\omega_r}{\omega_0} = \sqrt{1-n} = \nu_r \tag{2.23}$$

ν_r is named radial betatron frequency or radial tune. As it can be understood from Equation 2.22, to get a real solution and radial stability, field index must be smaller than 1. However, it has no lower bound.

Vertical stability conditions must also be checked. Equation of motion in vertical direction can be written as;

$$m\ddot{z} = qvB_x \qquad (2.24)$$

To solve Equation 2.24, B_x must be found. For this purpose, Ampere-Maxwell law can be used:

$$\nabla \times \vec{B} = \mu_0 \vec{J} + \mu_0 \varepsilon_0 \frac{\partial \vec{E}}{\partial t} \qquad (2.25)$$

Right hand side of Equation 2.25 becomes zero inside the vacuum chamber. Thus, Equation 2.26 is obtained.

$$\frac{1}{r}\left[\frac{\partial B_z}{\partial \theta} - \frac{\partial B_\theta}{\partial z}\right]\hat{r} - \left[\frac{\partial B_z}{\partial r} - \frac{\partial B_r}{\partial z}\right]\hat{\theta} + \frac{1}{r}\left[\frac{\partial r B_\theta}{\partial r} - \frac{\partial B_r}{\partial \theta}\right]\hat{z} = 0 \qquad (2.26)$$

Furthermore, $\frac{\partial B_z}{\partial \theta}=0$, $\frac{\partial B_r}{\partial \theta} = 0$ and $B_\theta = 0$ because of uniformity. Using these assumptions, Equation 2.26 is simplified to $\frac{\partial B_r}{\partial z} = \frac{\partial B_z}{\partial r}$. Then replacing r with x (because $r=r_0+x$) and using the field index, Equation 2.24 turns into Equation 2.30.

$$\frac{\partial B_x}{\partial z} = \frac{\partial B_z}{\partial x} = \frac{-nB_z(r_0)}{r_0} \qquad (2.27)$$

$$m\ddot{z} = -qv\frac{nB_z(r_0)z}{r_0} \qquad (2.28)$$

$$m\ddot{z} + qv\frac{nB_z(r_0)z}{r_0} = 0 \qquad (2.29)$$

$$m\ddot{z} + \omega_0^2 n z = 0 \tag{2.30}$$

Solution of the equation of motion is:

$$z = z_{max} \sin(\sqrt{n}\omega_0 t) \tag{2.31}$$

$$\omega_z = \omega_0 \sqrt{n} \tag{2.32}$$

$$\frac{\omega_z}{\omega_0} = \sqrt{n} = \nu_z \tag{2.33}$$

ν_z is named vertical betatron frequency or vertical tune. The vertical stability is only possible with a real solution. Therefore, in Equation 2.32, n must be greater than zero. In this case the complete transverse stability condition becomes $0 < n < 1$. It can be found by combining Equation 2.32 and Equation 2.22.

As it has been mentioned before, magnetic field is not exactly uniform in our case. Its z component slowly decreases with increasing r. Slowly decreasing magnetic field naturally provides a vertical focusing, named "weak focusing". And weak focusing is crucial for a classical cyclotron.
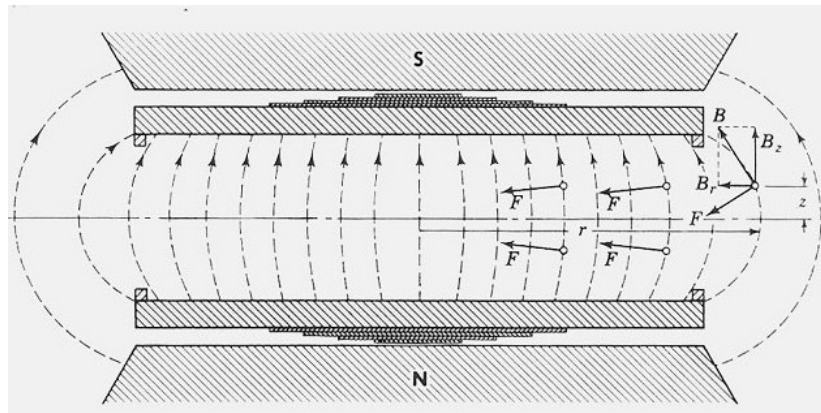
Figure 2.1. A visual for weak focusing [4].

Besides magnetic focusing, electrostatic focusing should also be considered. For the initial orbits electrostatic focusing has an important role. Robert Wilson dealt with this issue and showed that if the d/h increases, than ions become defocused. Here d is the separation between the dees and h indicates height of the dees. Therefore, d must be as small as possible to prevent defocusing of ions [11].

3. MAIN COMPONENTS OF THE CYCLOTRON

3.1. Iron Yoke

Iron yoke (H-shaped magnet) is a medium that magnetic field lines travel through. It has 2 magnetic poles. In our case, one of the pole is fixed to right side and the other is at the left side the of yoke.

The magnitude of the magnetic field is very important. Because greater magnetic field guarantees increasing the final energy of particles. Correlation between them can be seen from Equation 3.2.

$$v = \frac{qBr}{m} \tag{3.1}$$

$$K = \frac{mv^2}{2} = \frac{q^2 B^2 r^2}{2m} \tag{3.2}$$

$$1 \text{ MeV} = \frac{(1.6 \times 10^{-19} \text{ C})^2 B^2 (0.20 \text{ m})^2}{2 \times 1.67 \times 10^{-27} \text{ kg}} \tag{3.3}$$

$$B = 0.72 \text{ T} \tag{3.4}$$

The projected magnetic field is 0.72 T to obtain 1 MeV protons. Therefore, firstly, the magnetic field strength has been checked using Poisson SuperFish (PSF) simulation software. The two dimensional PSF model of H-magnet can be seen from Figure 3.1.
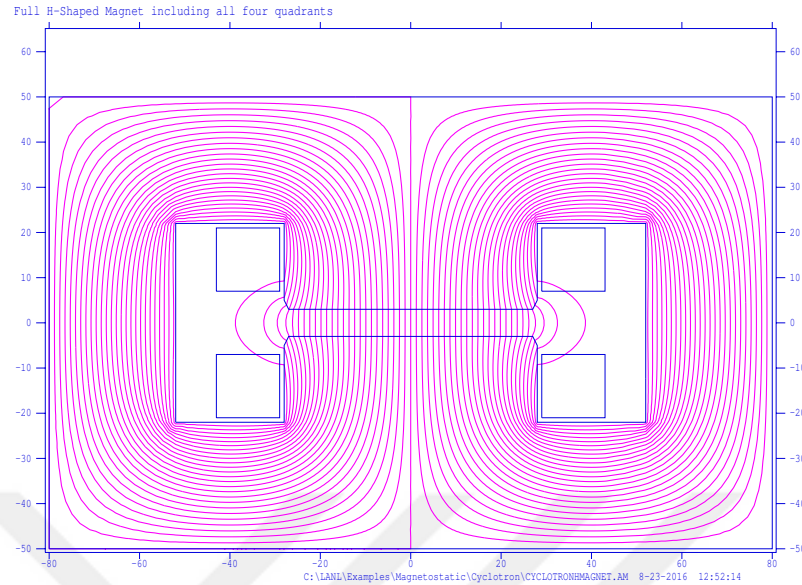
Figure 3.1. Poisson SuperFish model for B field in the H-magnet.

To get a denser magnetic field, construction material of H-magnet must have high magnetic permeability. For this reason, GJS 400-15 was preferred, as it " 400-15 is a spherical graphite cast iron with fully ferritic matrix" which has high magnetic permeability and low hysteresis loss [12]. (When a ferromagnet is magnetized by an external magnetic field even if removed, ferromagnet still stays magnetized. The additional power loss required for demagnetization called hysteresis loss.)

Hysteresis loss of GJS 400-15 is smaller than the other cast irons, as can be seen from Figure 3.2(a). Drawn with green, it has the smallest area enclosed by its B-H curve. Besides, as it is seen in Figure 3.2(b), the magnetic saturation of GJS 400-15 is higher than the other cast irons. High saturation level is another advantage of GJS 400-15 because saturation level limits the magnetic field B.
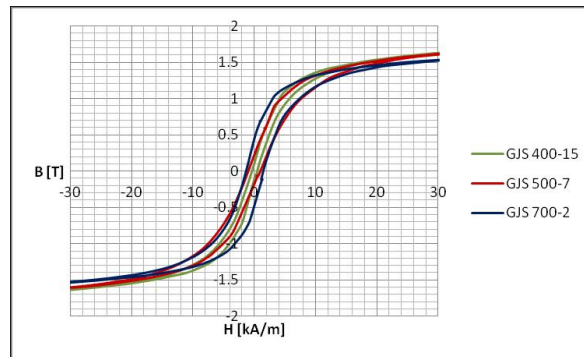
(a)
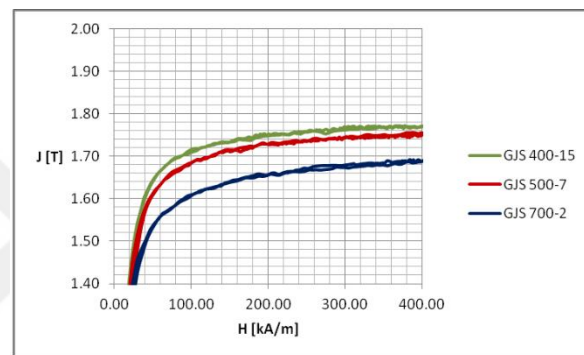
(b)

Figure 3.2. B-H curve and saturation levels of spherical graphite cast irons in (a),(b) respectively.

[12]

Besides, creating a uniform magnetic field is important for keeping constant the frequency of ions, $f = \dfrac{qB}{2\pi m}$. Therefore, chemical properties of the material used for the H-magnet must be identical everywhere to obtain a uniform magnetic field.

Ideal way of keeping the chemical structure of the iron homogeneous is to prepare and cast it in one sitting. In our case, iron was prepared in one go but casting had to be completed in two steps because appropriate casting mould size was not available.

Mechanical design of iron yoke was made in AutoCAD-3D 3.3. A list of its components are given in Table 3.1. Iron yoke can be opened from the part of T02. Openable part gets easier working on the vacuum chamber. The height, width and depth of iron yoke are 1300 mm, 1002 mm and 580 mm respectively.

Its total mass is approximately 5000 kg.

<table>
<tr><td>(a)</td><td>(b)</td></tr>
</table>
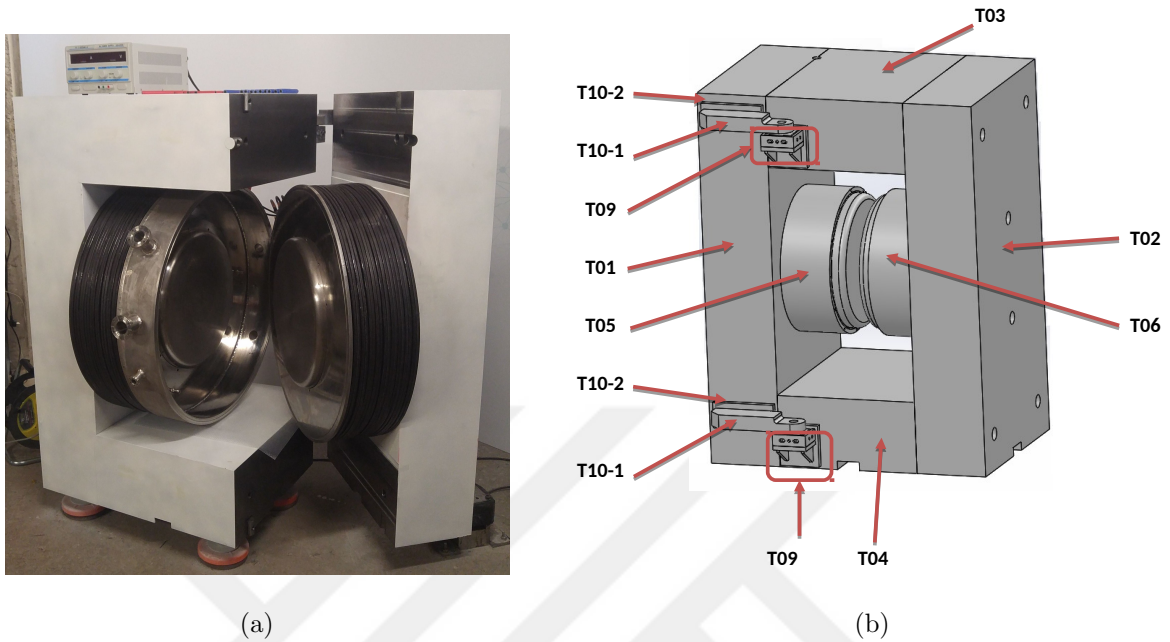
Figure 3.3. OZU Cyclotron and the list of its part in (a), (b) respectively.

Table 3.1. List of the Cyclotron parts.

CYCLOTRON PART LIST							
item no	position no	length (mm)	depth (mm)	height (mm)	mass(kg)	number of pieces	total mass(kg)
1	T01	250	580	1300	1,479.7	1	1,479.7
2	T02	250	580	1300	1,479.7	1	1,479.7
3	T03	502	580	250	571.4	1	571.4
4	T04	502	580	250	571.4	1	571.4
5	T05	255	0	520	416.6	1	416.6
6	T06	255	0	520	416.6	1	416.6
7	T09-1	10	60	95	0.4	4	1.8
8	T09-2	15	100	125	1.5	2	2.9
9	T09-3	10	140	150	1.6	2	3.3
10	T09-4	40	80	95	2.4	2	4.8
11	T09-5	40	100	125	3.9	2	7.9
12	T09-6	20	0	70	0.2	2	0.3
13	T10-1	10	90	225	1.6	2	3.2
14	T10-2	50	95	345	13	2	25.7
						Overall(kg)	4,985.3

Iron yoke was painted with rustproof spray paint to prevent oxidation. After painting, magnet coils were mounted over the magnetic poles.

3.2. Coils

Magnet coils have been constructed using annealed 8×8 mm copper square pipes. These pipes must be electrically insulated. Generally, fiberglass is used for insulation of coils but there is no opportunity to manufacture insulated hollow copper squared pipes in Turkey. Therefore, it was decided that pipes are wrapped in heat shrinkable tubes.

Firstly, coils were hanged on a custom-built coil suspender (Figure 3.4b) in order to coat them without deforming their circular shapes. To cover them, 12/6 mm heat shrinkable tubes(Woer RSFR-H, China) that endure up to 125 degrees Celcius were used.

Every package of heat shrinkable tube is 100 meters long but they had to be cut into pieces. After some trials, it is decided that 1 meter is the ideal length for covering the coils on the hanger. Each 1 meter long piece is then shaped into square in cross section. Once the shrink tube has been slided into position around the pipe, the next step is heating with hot air gun so that shrinkable tubes take the form of the copper pipes.
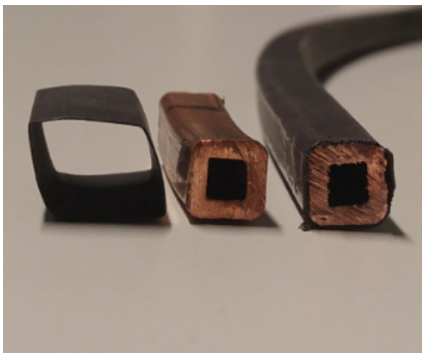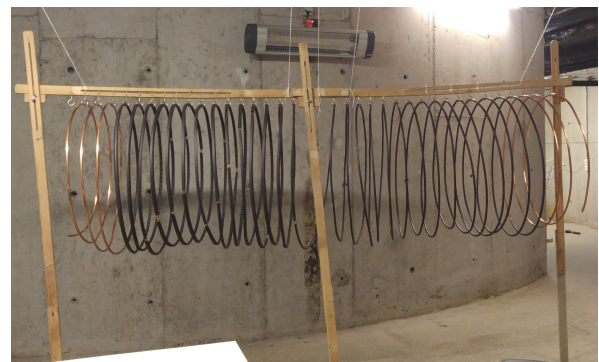
(a)   (b)

Figure 3.4. (a) A small piece of heat shrinkable tube, copper pipe and copper pipe covered with heat shrinkable tube. (b) Custom-built hanger of coils.

A table which turns around a pivot has been produced for winding the coils. The pivot was fixed into floor and a table was placed on it. Before winding, the center point of the coil along its length was determined and marked. It is started to wind from this center. After one half of the coil was spirally wounded to obtain the first pancake, epoxy was applied on the upper surface. The other half was wounded in the opposite direction. Thus, both ends of the coil came out in the same direction, enabling ease ofuse as water inlet and outlet.
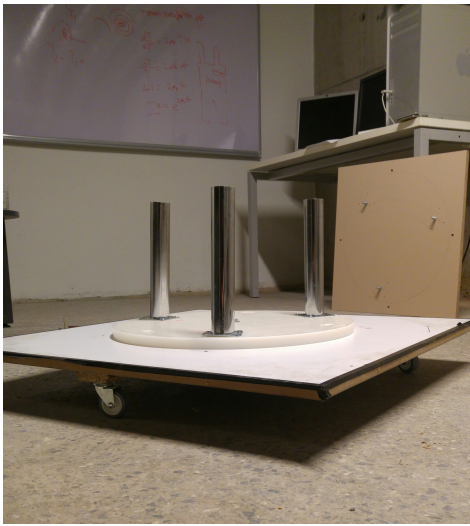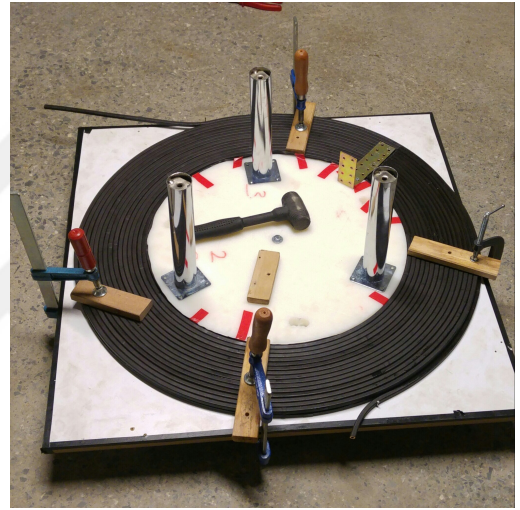
(a)   (b)

Figure 3.5. Coil winding table and one of the double pancakes in (a), (b) respectively.

At the end, 18 double pancakes, each of which consists of 30 coil windings was made in our laboratory. 9 of them was mounted to right pole and the others to left pole.

Coil resistance of each double pancake was calculated easily using Ohm's Law. Dividing the applied voltage to current read gives resistance of a coil. They have almost same values around 0.028 Ω(at 1.1 V). Resistance of the full pancake(18 double pancakes) can be calculated as $18 \times 0.028\ \Omega = 0.50\ \Omega$. It is consistent with the measurements (Figure 3.6). The small difference stems from the contact resistance.

Voltage(V)	Current(A)
0.6	1.0
1.2	2.0
1.9	3.0
2.6	4.0
3.2	5.0
3.8	6.0
4.5	7.0
5.1	8.0
5.7	9.0
6.3	10.0
7.0	11.0
7.5	12.0
8.2	13.0
8.9	14.0
9.4	15.0
10.1	16.0
10.7	17.0
11.3	18.0
11.8	19.0
12.3	20.0
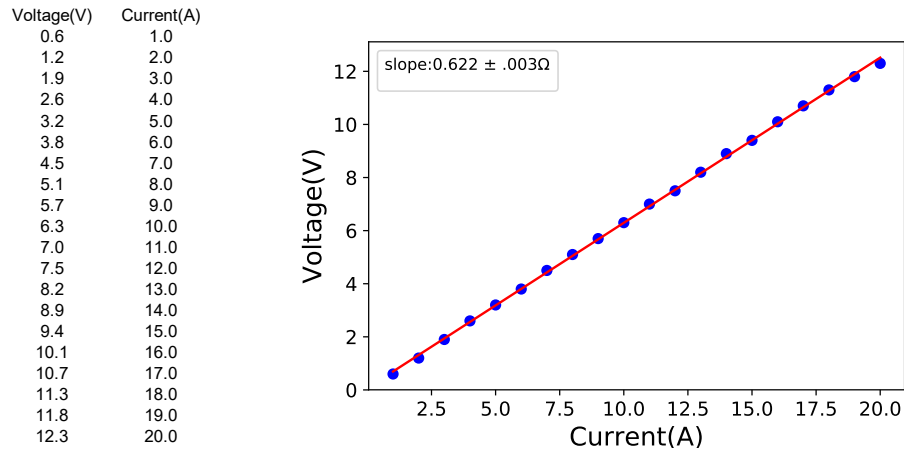
(a)   (b)

Figure 3.6. Voltage vs Current plot with linear fit data.

3.3. Vacuum Chamber

Ions can only be accelerated in a high vacuum chamber. Vacuum chamber consists of a chamber and lid which are made of high quality stainless steel 316L. Inner and outer radii are 46.0 cm and 78.0 cm, respectively.
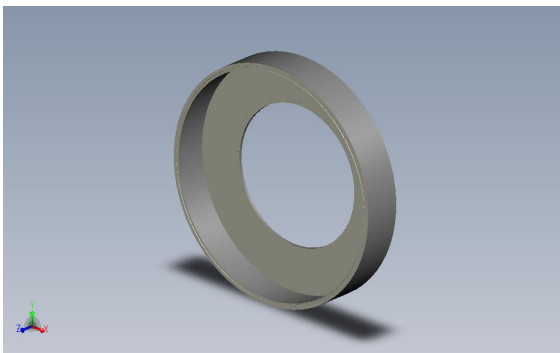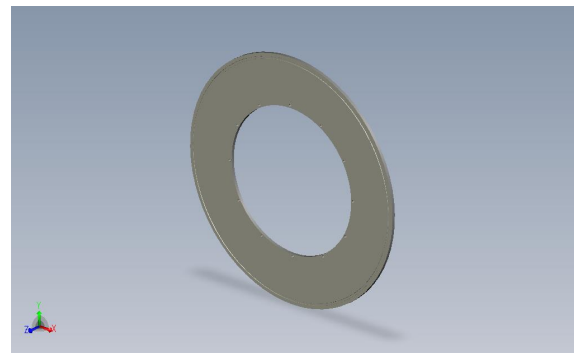
(a)   (b)

Figure 3.7. AutoCAD drawing of vacuum chamber and its lid in (a), (b) respectively.

There is a groove on the lid for a viton o-ring since viton o-ring is a good vacuum seal. Also, two copper electrodes(dees) and an ion source will be mounted in the chamber (Figure 3.8).
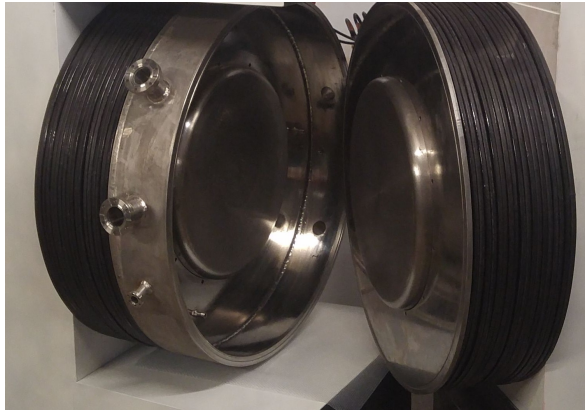
Figure 3.8. Vacuum chamber of OZU Cyclotron

In addition, 6 conflat flange ports have been welded on the vacuum chamber. 4 of the flanges are 2.75 inches in diameter and others are 1.33 inches. These ports will connect the vacuum chamber to different subsystems such as a hydrogen gas inlet tube, RF signal generator, RF matching box, a vacuum pump, and filament leads. Furthermore, there is a viewport on the chamber to observe the inside of the chamber.

A turbo molecular pump will use to vacuum inside of the chamber. The ultimate pressure of turbo molecular pump is 7.5×10^{-8} torr and pumping speed at 50 Hz is 0.75 m^3/h. It is deemed sufficient because approximately 10^{-5} torr is enough for the expected mean free path, 31.69 m :

$$\lambda = \sum_{n=1}^{N} \pi R_n = \frac{\pi}{B} \sqrt{\frac{2m\Delta V}{q}} \sum_{n=1}^{N} \sqrt{n} \tag{3.5}$$

λ: Mean free path

n: Number of semi circular revolution

R: Radius of curvature

B: Magnetic field strength (assumed that 0.68 T)

V: Applied voltage (5000 V)

M: Mass of proton (1.67×10^{-27} g)

q: Charge of proton (1.67×10^{-19} C)

(a)   (b)

Figure 3.9. Turbomolecular air pump and conflat flanges in (a), (b) respectively.

For design of the dees, Houghton Cyclotron was patterned which has 0.6 d/h ratio where d is gap between the dees and h is the height of the dees [13]. It was decided that d is 2.0 cm and h is 3.3 cm for OZU Cyclotron.

3.4. Ion Source

An ion source is essential to produce ion beam between the dees. There are several types of ion sources such as filament ion source, chimney ion source and PIG(penning ionization gauge) ion source. A chimney ion source was preferred in OZU Cyclotron, see Figure 3.10 (a) because of ease of use and ease of production cost.

Obtaining a focused ion beam depends on some factors. Stability of the first orbit is one of them. Since the magnetic field focusing is weaker for the initial orbits, pullers will be mounted on the dee aligned vertically with the aperture of chimney, see Figure 3.10 (b). This is very important because if the initial launch angle of ions becomes higher than desired, ions can hit the surface of the dees.

(a)   (b)

Figure 3.10. Chimney and pullers in (a), (b) respectively [14].

It was decided to accelerate protons therefore; hydrogen gas must be ionized by electrons emitted from a hot filament. In our case, thoriated tungsten will be used as a filament.

3.5. RF System

To accelerate the ions, an alternating voltage must be applied to the dees. Frequency of OZU Cyclotron is in the domain of high frequency(HF) which is 2-30 MHz. An RF signal generator (Figure 3.11) will be used to create the desired voltage signal. The generator will provide 1mW power output at 0 dBm, and a custom-built RF power amplifier will increase the power up to 1.1 kW, to be transferred to the cyclotron.

Figure 3.11. The signal generator selected for providing the input signal:
RIGOL-DG4102.

Maximum power transmission from RF signal generator to the cyclotron is possible with matching the impedance of cyclotron and the impedance of RF source. In case of a mismatch, some power reflects back. Power reflection decreases the efficiency of the system and can also damage the electronic devices.

Power reflection creates standing wave in the transmission line. Reflection amount is determined by means of voltage standing wave ratio (VSWR). If the VSWR value equals to 1 that means no power reflects back.

$$\text{VSWR} = \frac{V_{max}}{V_{min}} = \left| \frac{V_{fwd} + V_{ref}}{V_{fwd} - V_{ref}} \right| \tag{3.6}$$

VSWR can also be expressed as $\text{VSWR} = \frac{1+|\Gamma|}{1-|\Gamma|}$ in terms of the reflection coefficient $\Gamma = \frac{V_{ref}}{V_{fwd}}$. Furthermore, expanded form of the reflection ratio is $\Gamma = \left| \frac{Z_{load} - Z_{source}}{Z_{load} + Z_{source}} \right|$. As it is seen, if Γ is zero then VSWR becomes unity. That means $| Z_{source} |$ equals to $| Z_{load} |$ where Z_{load} is the impedance of the cyclotron and Z_{source} is the impedance of the RF signal generator.

The RF system has a negligible resistance value therefore it has been modelled as an LC circuit. Dee shaped electrodes act as a capacitors. For calculation of the cylotron capacitance, parallel plate capacitor approximation can be used. Capacitance of a paralel plate capacitor is calculated using C= $\frac{\epsilon_0 A}{d}$ formula.

Firstly, area of the capacitor should be calculated. Radius of the Dee-1(R_{D1}) is 0.210 m and the radius of Dee-2(R_{D2}) is 0.200 m. R_{D2} is slightly smaller because ions will be extracted from there.

ϵ_0: Vacuum permittivity (8.85×10^{-12} F/m)

A: Area of plate

d: Gap between the dees (0.02 m)

h: Height of the dees (0.034 m)

x: Distance between the pole chamfer and dee (0.005 m)

$$A_1 = \frac{1}{2}\pi(0.0210\,\text{m})^2 = 0.069\,\text{m}^2 \quad A_{1side} = \pi(0.210\,\text{m})(0.034\,\text{m}) = 0.022\,\text{m}^2$$

$$A_2 = \frac{1}{2}\pi(0.200\,\text{m})^2 = 0.063\,\text{m}^2 \quad A_{2side} = \pi(0.0200\,\text{m})(0.034\,\text{m}) = 0.021\,\text{m}^2$$

$$C_{1top} = \frac{\epsilon_0 A_1}{x} = 122\,\text{pF} \quad C_{2top} = \frac{\epsilon_0 A_2}{x} = 111\,\text{pF}$$

$$C_{1bottom} = \frac{\epsilon_0 A_1}{x} = 122\,\text{pF} \quad C_{2bottom} = \frac{\epsilon A_1}{x} = 122\,\text{pF} \tag{3.7}$$

$$C_{1side} = \frac{\epsilon_0 A_{1side}}{2x} = 19.9\,\text{pF} \quad C_{2side} = \frac{\epsilon_0 A_{2side}}{2x} = 18.9\,\text{pF}$$

$$C_{1top} + C_{1bottom} + C_{1side} = 265.07\,\text{pF} \quad C_{2top} + C_{2bottom} + C_{2side} = 241\,\text{pF}$$

$$\frac{1}{C_{total}} = \frac{1}{265\,\text{pF}} + \frac{1}{241\,\text{pF}} \quad C_{total} = 126\,\text{pF}$$

To accelerate ions, frequency of the LC circuit must be matched with the frequency of ions. Frequency of ions and capacitance value of the dees are calculated in Equations 3.7 and 3.19, respectively. Using these values, the matching inductance can be calculated as:

$$f_0 = \frac{1}{2\pi\sqrt{LC}} \tag{3.8}$$

$$L = \frac{1}{4\pi^2 f_0^2 C} = \frac{1}{4\pi^2 (10 \times 10^6\,\text{MHz})^2 (126 \times 10^{-12}\,\text{F})} = 2\,\mu H \tag{3.9}$$

3.5.1. Oscillation Frequency

OZU Cyclotron is a classical cyclotron because of its energy scale. For the protons having 1 MeV kinetic energy, Lorentz factor becomes 1.001 (Equation 3.12).

$$K_{rel} = (\gamma - 1)mc^2 \tag{3.10}$$

$$1MeV = (\gamma - 1)(938.28)\,\frac{\text{MeV}}{\text{c}^2}\text{c}^2 \tag{3.11}$$

$$\gamma = 1.001 \tag{3.12}$$

As long as the non-relativistic classical formulas are applicable, it is easy to show that the rotation frequency of ions does not change as they move to outer orbits gradually. It is also shown in Equation 3.15 using kinetic energies of ions for 2 different orbits in Equation 3.13 and Equation 3.14.

$$K_1 = \frac{mv_1^2}{2} = \frac{q^2 B^2 r_1^2}{2m} \tag{3.13}$$

$$K_2 = \frac{mv_2^2}{2} = \frac{q^2 B^2 r_2^2}{2m} \tag{3.14}$$

Here, B and q are constant. As discussed before, m is also constant because our cyclotron operates in the non-relativistic region. Dividing these two equations gives;

$$\frac{(v_1)^2}{(v_2)^2} = \frac{(r_1)^2}{(r_2)^2} \quad \text{then;} \quad \frac{v_1}{r_1} = \frac{v_2}{r_2}. \quad \text{v} = 2\pi fr \text{ is also known therefore } f_1 = f_2 \tag{3.15}$$

To calculate expected frequency of the ions, the magnetic field was calculated then substituted into the formula below.

$$f_0 = \frac{qB}{2\pi m} \tag{3.16}$$

$$\oint H.\,dx = \frac{Bg}{\mu_0} + \frac{B_{iron}L_{iron}}{\mu_{iron}} = NI \tag{3.17}$$

N: number of turns

g: 0.05 m distance between the pole faces

μ_0 : permeability of vacuum

μ_{iron} : permeability of iron

Permeability of iron is much bigger than the vacuum permeability therefore second term on the right side of Equation 3.17 can be neglected:

$$
\begin{aligned}
B &= \frac{\mu_0 N I}{g} \\
&= \frac{(1.26 \times 10^{-6} \text{ H/m})(540)(50 \text{ A})}{0.05 \text{ m}} = 0.68 \text{ T}
\end{aligned}
\tag{3.18}
$$

B$_z$ value was inserted into the Equation 3.19 thus expected ion frequency was found as 10 MHz.

$$
f_0 = \frac{qB}{2\pi m} = f_0 = \frac{(1.602 \times 10^{-19})(0.68)}{2\pi 1.672 \times 10^{-27}} = 10 \text{ MHz}
\tag{3.19}
$$

3.6. Cooling System

To create a magnetic field, a direct current is to be applied to coils. This current heats up the copper pipes; therefore, a cooling system is needed to regulate the temperature. For this purpose, cold water is flowed through the copper coils.

Inevitably, there would be a heat transfer from pipes to water; hence heated water must be chilled. Heated water will be drained with the help of 18 red water manifolds and collected in a water tank. Finally, water will be chilled by a commercial heat exchanger as shown in Figure 3.12 and returned back to magnet coils. Cold water are to be delivered to the coils by 18 blue water manifolds (Figure 3.13).
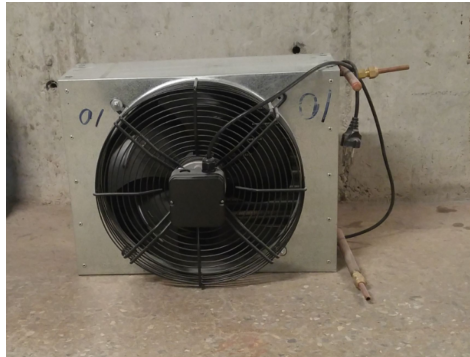
Figure 3.12. Heat exchanger.
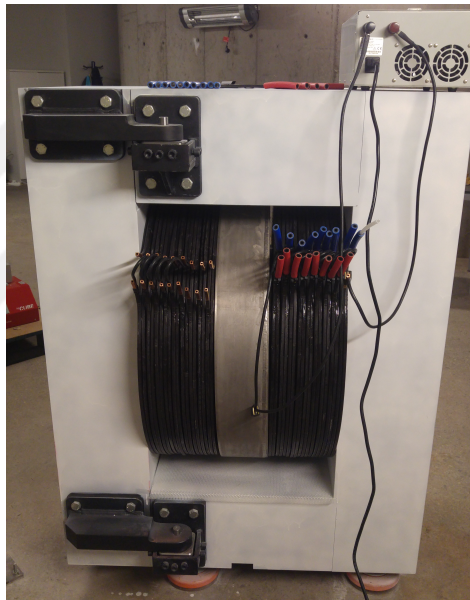
Figure 3.13. Water manifolds.

There are 3 types of fluid flow in a pipe, namely laminar, transient and turbulent. The dominant factor in determining the flow type of a fluid is Reynolds number. Reynolds number is $Re = \dfrac{vd}{\nu}$ where v is the velocity of water, ν is the kinematic viscosity of water and d is the water circuit diameter. If the Reynolds number is less than 2000 then flow type becomes laminar. For a turbulent flow Reynolds number must be greater than 4000. And flow type is transient when it is $2000 < Re < 4000$.

In our case, flow type should be turbulent because the fastest heat exchanging from copper pipes to water can be possible with a chaotic motion of water molecules. For that reason, the turbulent flow conditions must be calculated.

Table 3.2 includes all of the flow parameters.

Table 3.2. Flow parameters.

v(m/s)	Re(10^3)	q(mL/sec)	q(L/hr)	ΔT(C)	ΔP(bar)	qtotal(L/sec)
0.34	1.19	5.37	19.34	2.39	0.50	0.10
0.51	1.80	8.15	29.33	1.58	1.00	0.15
0.65	2.29	10.37	37.33	1.24	1.50	0.19
0.77	2.72	12.29	44.25	1.04	2.00	0.22
0.88	3.10	14.02	50.47	0.92	2.50	0.25
0.98	3.45	15.60	56.17	0.82	3.00	0.28
1.07	3.78	17.08	61.48	0.75	3.50	0.31
1.15	4.09	18.47	66.48	0.70	4.00	0.33
1.24	4.38	19.78	71.21	0.65	4.50	0.36
1.31	4.65	21.03	75.72	0.61	5.00	0.38
1.39	4.92	22.23	80.03	0.58	5.50	0.40
1.46	5.17	23.38	84.18	0.55	6.00	0.42
1.53	5.42	24.50	88.19	0.52	6.50	0.44
1.60	5.66	25.57	92.06	0.50	7.00	0.46
1.66	5.89	26.61	95.81	0.48	7.50	0.48
1.73	6.11	27.63	99.46	0.46	8.00	0.50
1.79	6.33	28.61	103.01	0.45	8.50	0.52
1.85	6.54	29.57	106.47	0.43	9.00	0.53
1.91	6.75	30.51	109.84	0.42	9.50	0.55
1.96	6.95	31.43	113.14	0.41	10.00	0.57

While water flows inside the coils, the pressure drop occurs. It is caused by friction between the water molecules and pipe wall, friction between the water molecules itself, elevation or elements of the pipeline. Pressure drop can be calculated using Darcy Weisbach formula see Equation 3.20.

$$\Delta P = \frac{f l \delta v^2}{2d} \tag{3.20}$$

Where l and d are water circuit length and diameter, respectively. v is water velocity, δ is water mass density and f is friction factor. l, d and δ are given. Velocity of water and friction factor must be calculated. Friction factor of a turbulent flow, f, can be figured out using Colebrook formula, see Equation 3.21.

$$\frac{1}{\sqrt{f}} = -2 \log_{10}(\frac{K}{3.7} + \frac{2.51}{Re} \frac{1}{\sqrt{f}}) \tag{3.21}$$

Here, K is the relative roughness constant and K=$\frac{\epsilon}{D}$. Re=$\frac{vd}{\nu}$. Reynolds number should be greater than 4000 for the turbulent flow. As it is seen from Figure 3.14, Reynolds number has been chosen as 5000, guaranteeing the flow type is turbulent. Right upper quadrant of the figure guarantees that flow type is turbulent.
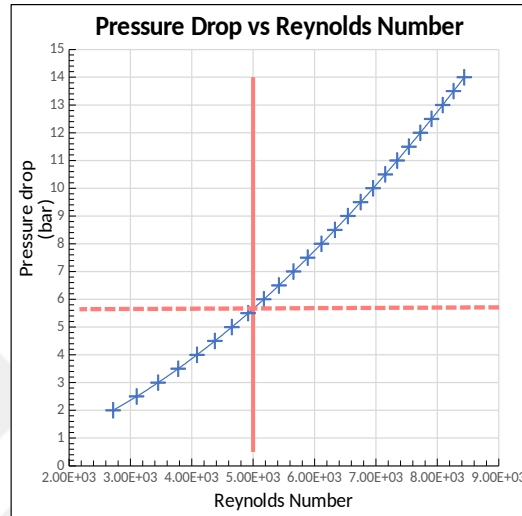
Figure 3.14. Pressure drop vs Reynolds number.

When flow rate is 22 mL/s, Reynolds number becomes approximately 5000. Under these conditions, for every second temperature of water inside the coils, 0.40l, increases of 0.58 degrees Celcius while cyclotron operates at 50A DC current. To overcome temperature increasing, a commercial heat exchanger was preferred [15]. However, in future for 100A a professional chiller unit will be required.

4. ANALYSIS

4.1. Magnetic Field Simulations

Magnetic field is responsible from both focusing and bending the ions in a circular path. It is almost but not exactly uniform. Going away from the center, magnitude of the z component of the magnetic field, B_z, slightly decreases. Therefore, a restoring force is generated on the particles. As previously mentioned, decreasing magnetic field provides weak focusing which keeps ions in the orbit. For this reason, magnetic field must be mapped before designing the H-shaped magnet to check weak focusing conditions (Equations 2.22 and 2.32).

Firstly, Poisson Superfish 2D simulation was used to control whether the magnetic field is as desired or not [16]. The model given by PSF is suitable for understanding roughly the behavior of magnetic field and its uniformity. However, PSF assumes that the geometry is cylindrically symmetric. In our case, H-shaped magnet does not have cylindrical symmetry. Therefore, another simulation tool is required for making 3D magnetostatics analysis.

Although finite element method (FEM) based simulations are usually used for this purpose, a software package Radia that uses boundary integral method was preferred because of financial reasons [17]. Furthermore, it is an advantage that Radia is interfaced with Mathematica.

Firstly, iron yoke, magnet coils and magnetic poles were constructed in Radia with their true sizes and characteristics. Iron yoke consists of several segments such as corners(positive and negative), horizontal segment between the corners and vertical end segments(positive and negative). Therefore, each segment was defined separately (Figure 4.1).
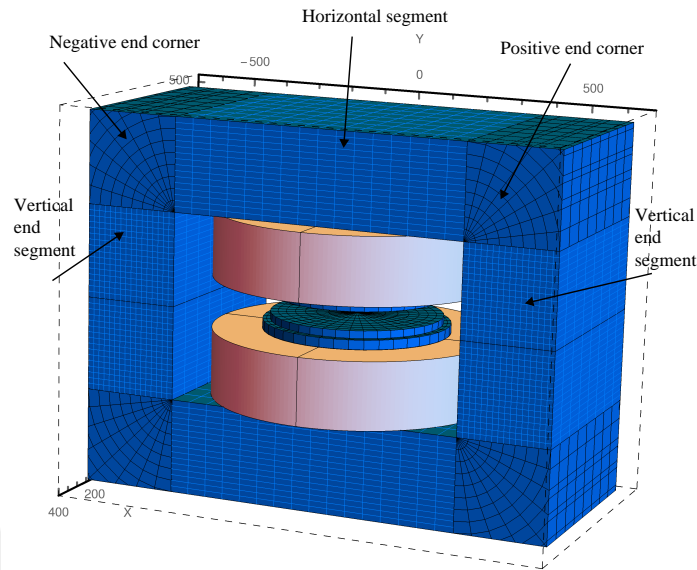
Figure 4.1. Meshed iron yoke with Radia.

Radia creates a symmetry of the object with respect to given symmetry axis. In our case, y axis was chosen as an axis of symmetry. Besides, design parameters and material properties of the H-magnet were also inserted to Radia.

Consequently, magnetic field values have been obtained at discrete points by Radia. After the magnetic field values have been obtained for every point, a CSV(comma separated value) file was created for the region between the pole faces that includes position of ion in x, y, z and corresponding magnetic field values as B_x, B_y, B_z. Using the CSV file, components of the simulated magnetic field plotted as seen in Figures 4.2 and 4.3.

(a)

(b)

(c)

(d)
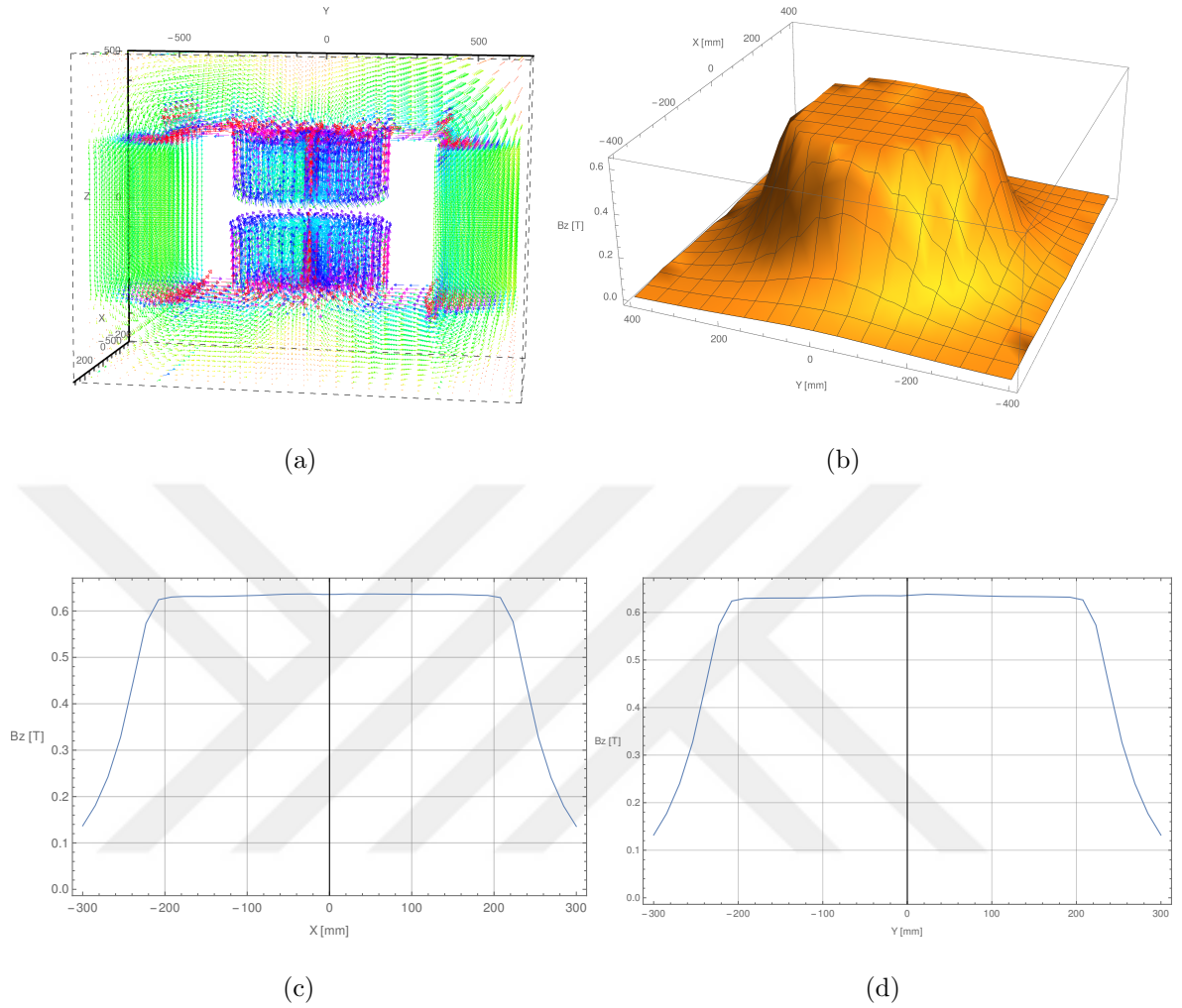
Figure 4.2. Magnetic field simulations computed with Radia. Magnetization, 3D B_z, B_z with changing x and B_z with changing y in (a), (b), (c), (d) respectively.
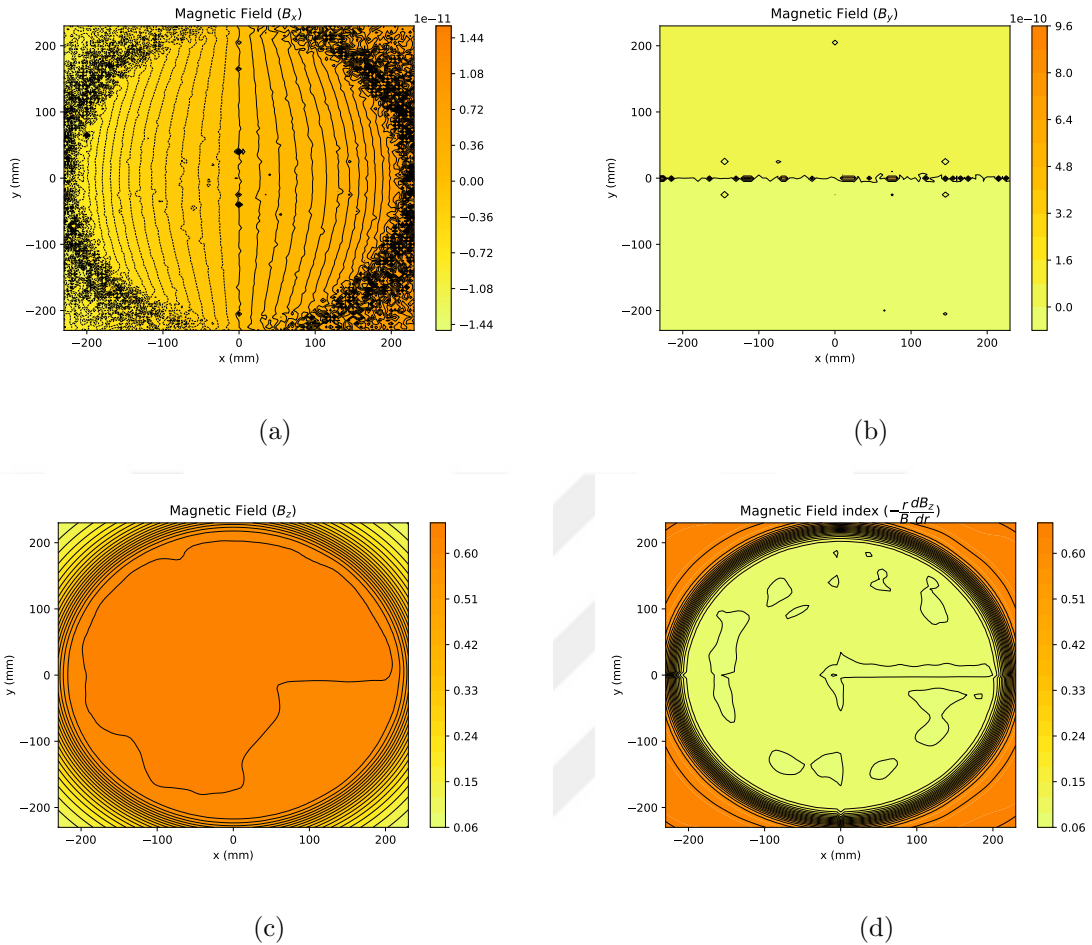
Figure 4.3. Magnetic field simulations and field index simulated with Python. x, y, z components in (a), (b), (c) respectively, field index shown in (d).

It can be concluded that z component of the magnetic field (B_z) is almost uniform as expected see Figure 4.2 and 4.3(c).

Beside the magnetic field, field index values have also been checked in the median plane. To meet the weak focusing conditions, (Equations 2.22 and 2.32), the field index must take the values between 0 and 1. In case it is 0, z component of magnetic field is regarded as uniform. On the other hand, a positive value up to 1 indicates slowly-decreasing magnetic field. According to simulation results in Figure 4.3(d), field index takes values between 0 and 1 as desired.

Contours seen in Figure (c) and (d) are computational artifacts.

4.1.1. Measurement of the z component of the Magnetic Field

The values of the z component of the magnetic field was measured in the median plane. A hall probe, connected to the teslameter, was mounted on the ruler for measuring B_z values [18].

Figure 4.4. Teslameter and hall probe.

The target current is 50 A. 50 A was applied to coils but the teslameter (PHYWE, 13610-90, Germany) is insensitive to the decimal changes in this scale. Therefore, magnetic field values were measured for 5 A, 10 A and 15 A at 4 cm intervals and 2 cm intervals respectively, then a linear fit was performed for each coordinate (Figure 4.5). As it can be seen from Equation 4.1, relation between B and the current is as expected. The coordinate of the outlier is $(-8,16)$ cm, hence it is 17.9 cm away from the center of the magnet.
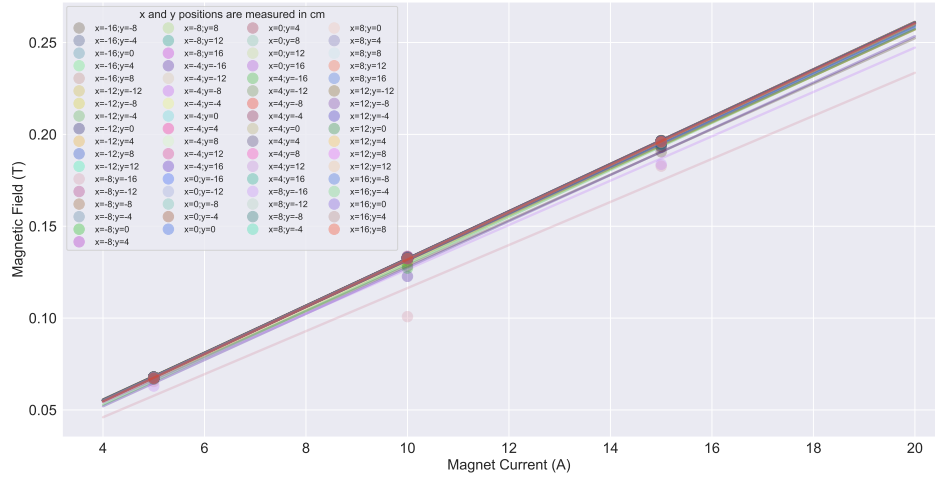
Figure 4.5. Magnetic field vs magnet current.
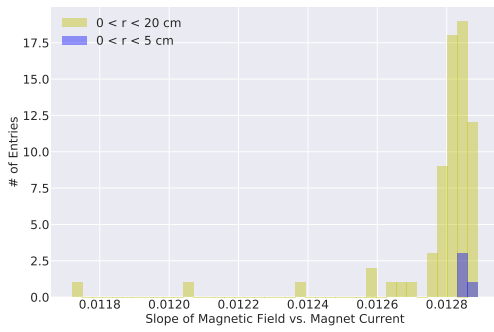
(a)
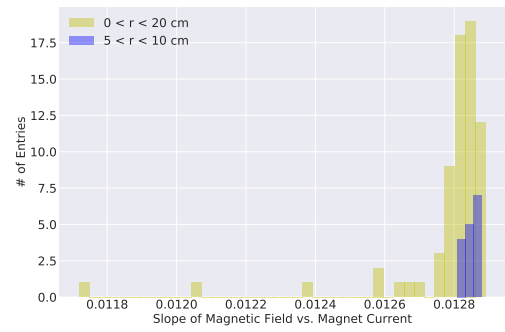
(b)
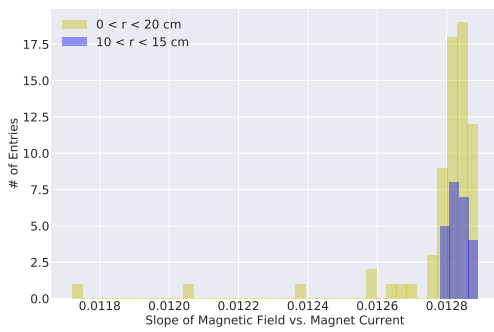
(c)
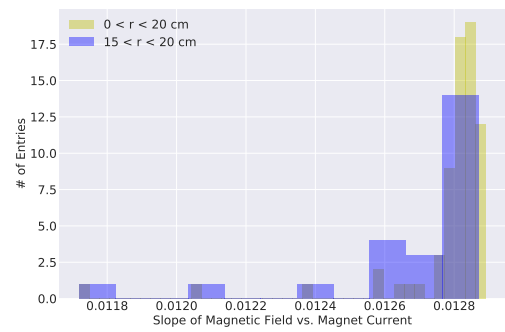
(d)

Figure 4.6. Histogram of the slope of magnetic field vs magnet current.

Figure 4.6 has been created with the slope values of Figure 4.5 for every measurement point at z=0 plane with $0 < r < 5$, $5 < r < 10$, $10 < r < 15$ and $15 < r < 20$. Most values in the dataset aggregate around 13×10^{-3} (Figure 4.6) as expected:

$$\frac{B}{I} = \frac{\mu_0 N}{g} = \frac{(1.26 \times 10^{-6} \text{ H/m})(540)}{0.05 \text{ m}} = 13.6 \times 10^{-3} \text{ T/A} \tag{4.1}$$

Furthermore, the magnetic field map has been created using the magnetic field values at 15 A (Figure 4.7). The map shows that the magnetic field between the pole faces is almost uniform as desired.
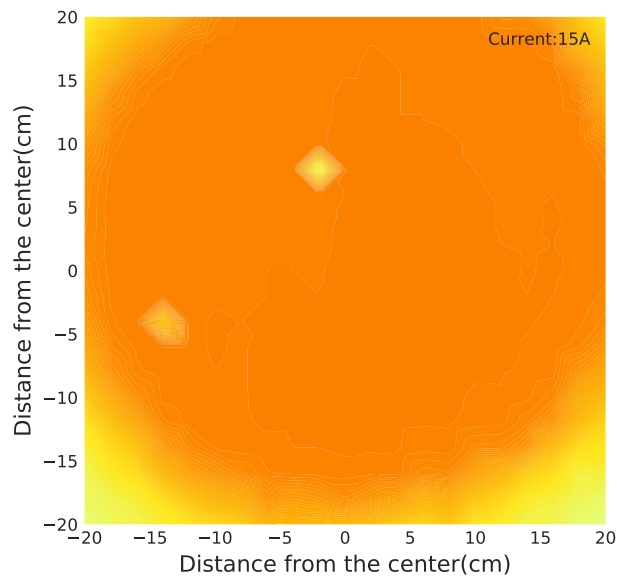
Figure 4.7. B_z map of the region between the pole faces at 15 A.

4.1.2. Ion Path Simulation

In a cyclotron, the ions are expected to move along a circular (rather helical) path. Once a magnetic field is available, an ion path simulation is required to foresee whether they indeed as expected. For this purpose, first a Modified Euler Method has been implemented in path to compute positions and velocities of ions (Equation 4.2). Modified Euler Method is a midpoint integration method.

It is also a type of 2nd order Runge Kutta Method.

$$
\begin{aligned}
\frac{dr}{dt} &= f(t,r) = v \quad r(t_n) = r_n \\
r_{n+1} &= r_n + k_2 \Delta t \\
k_1 &= \Delta t f(t_n, r_n) \quad k_2 = \Delta t f(t_n + \Delta t/2, r_n + k_1 \Delta t/2) \\
r_{n+1} &= r_n + \Delta t f(t_n + \Delta t/2, r_n + k_1 \Delta t/2) + O((\Delta t)^3)
\end{aligned}
\tag{4.2}
$$

However, results of the Modified Euler Method are found to be unreasonable. Although ions are exposed to same high voltage between the dees, as it can be seen from Figure 4.8, energy increments turn out to be different for each time interval. To get a realistic energy graph, time intervals should be decreased. However, the corresponding increase in the number of steps leads to very long computation times, since this is a CPU intensive calculation.
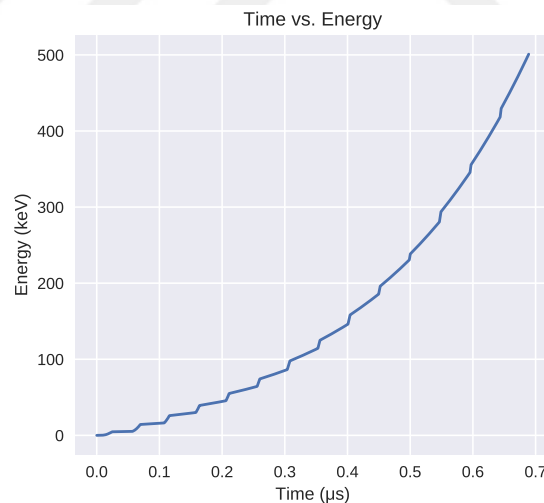
Figure 4.8. Energy vs time graph by Modified Euler Method with Δt= 0.83 ns.

Therefore, 4th order Runge Kutta Method, a more accurate approximation method, has been selected simulate the ion path.

Runge-Kutta Method has 2 more steps than the midpoint method(Equation 4.3). It calculates each next step using previous information and four evaluations.

Furthermore, 4th order Runge Kutta Method (RK4) has 5th order error whereas Modified Euler Method has 3rd order error. So, instead of taking many more steps and consuming CPU power, RK4 has been preferred as a more practical method.

RK4 can compute acceleration, velocity and displacement by using the given force and position of the particle. In our case, RK4 uses the previous position and velocity of ions to estimate the next position and velocities. According to 4th order Runge Kutta Method, $r_{n+1} = r_n + k$, therefore k needs to be calculated. Each of the "k" functions computes the slope of f (x, y) at four different points in the evaluation interval, thereby allowing us a more accurate calculation of how much the function changes between evaluation points. The algorithm gives more weight to the slopes in the middle of the interval (k2 and k3) and less weight to the slopes at the beginning (k1) and end (k4) of the interval [19].

$$
\begin{aligned}
&\frac{dr}{dt} = f(t,r) = v \quad r(t_n) = r_n \\
&k_1 = \Delta t f(t_n, r_n) \quad k_2 = \Delta t f(t_n + \Delta t/2, r_n + k_1/2) \\
&k_3 = \Delta t f(t_n + \Delta t/2, r_n + k_2/2) \quad k_4 = \Delta t f(t_n + \Delta t, r_n + k_3) \\
&k = 1/6(k_1 + 2k_2 + 2k_3 + k_4) \\
&r_{n+1} = r_n + 1/6(k_1 + 2k_2 + 2k_3 + k_4) + O((\Delta t)^5)
\end{aligned} \tag{4.3}
$$

(a)

(b)   (c)
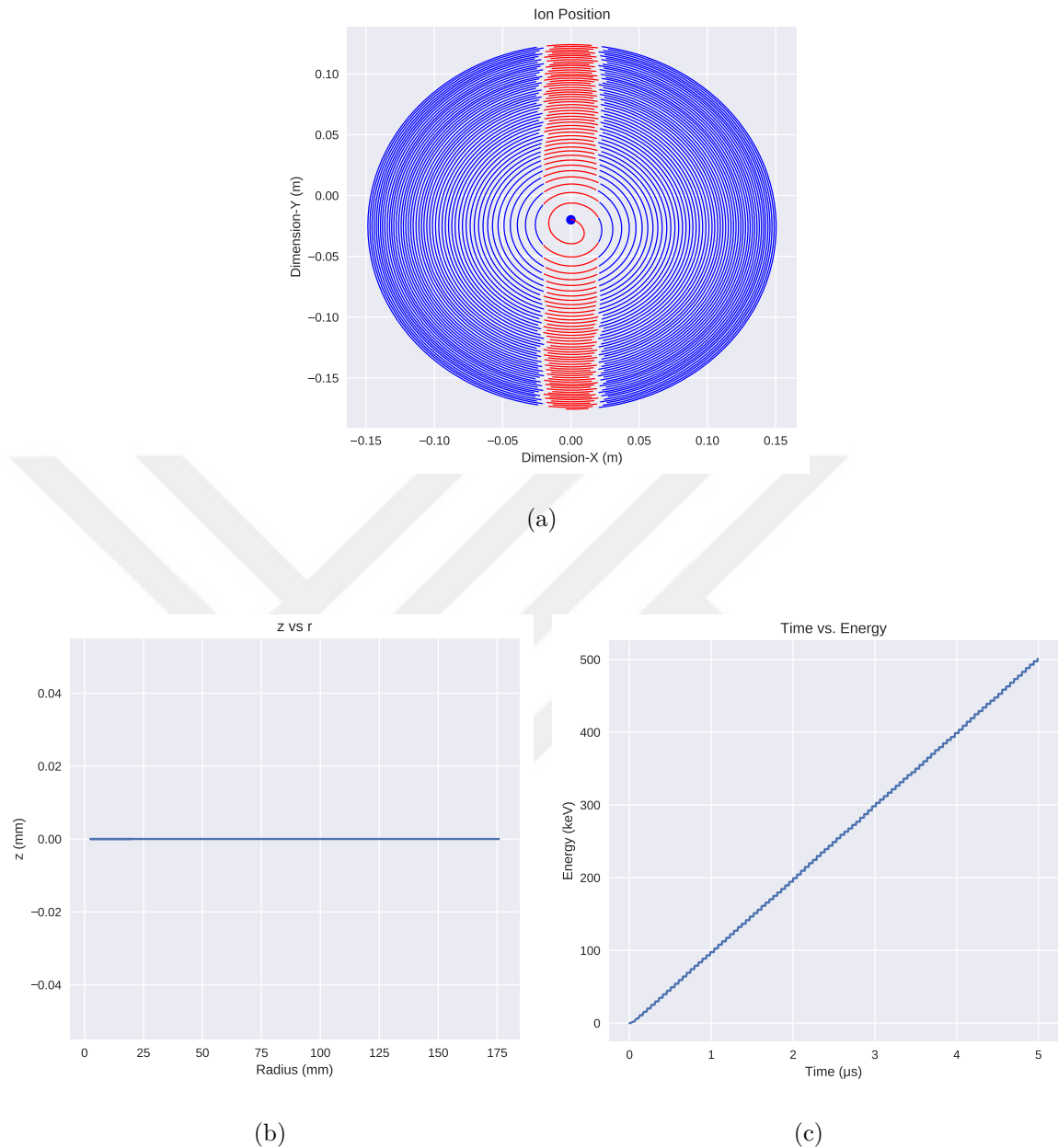
Figure 4.9. Ion path, z with changing r and energy changing with time at constant B value in (a), (b), (c) respectively.

In case of constant magnetic field, ion path is seen to agree with expectations from the theory. Also, energy of ion equally increases linearly this time as well (Figure 4.9). Therefore, these results show that RK4 works well.

However, for a more realistic simulation of an actual cyclotron, the magnetic field values must be computed and inserted into computation everywhere between the poles.

For that reason, the volume between the poles meshed and small bounding cubes have been created in it (Figure 4.10).
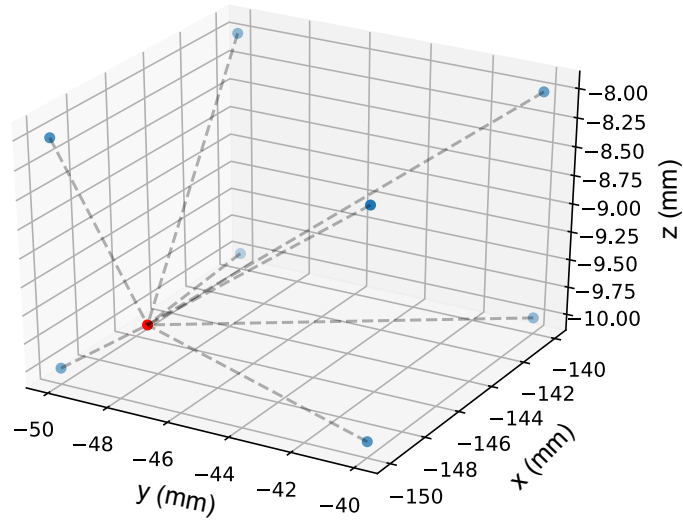
Figure 4.10. Bounding box.

Then, the magnetic field values can be extrapolated were calculated for every point of space using the magnetic field values at the corners of the bounding cubes with inverse distance weighting method. Finally, the magnetic field values are used in the ion path simulation.
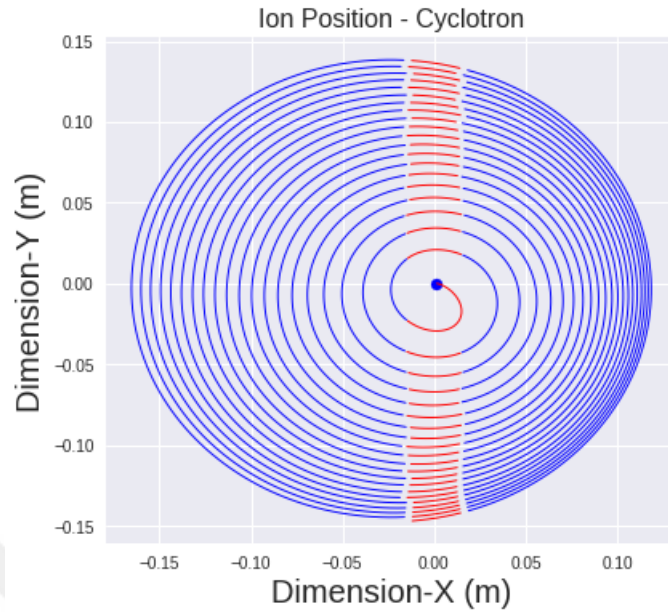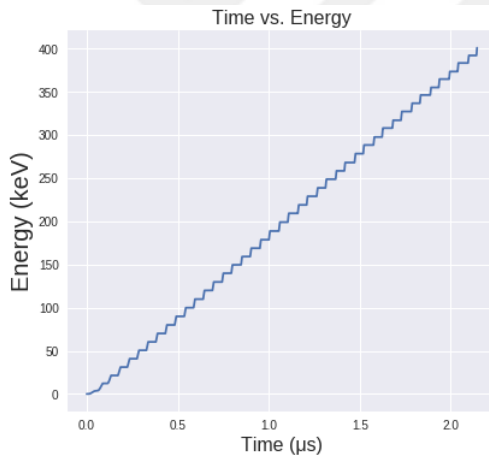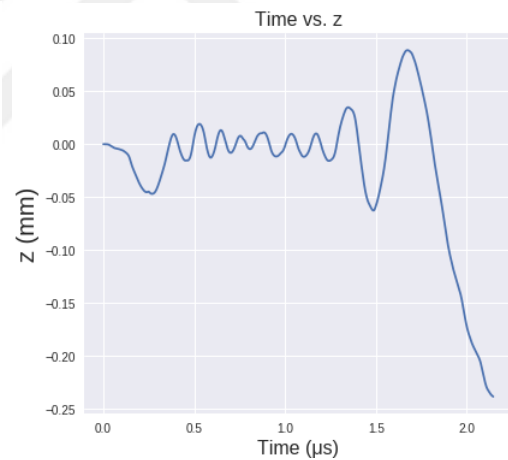
Figure 4.11. Energy of ions, betatron oscillations and ion path simulated with Python, in (a), (b), (c) respectively.

As it can be seen from Figure 4.11, ion path is expectedly helical but its center has shifted to right. This shift can be a result of initial velocity or launch angle of ions because pullers are at right in our design.

Small oscillations in Figure 4.11(b) are called betatron oscillations. Betatron oscillation is oscillation of ions around their equilibrium orbit that can be observed only in a cyclic accelerator.

In addition, Radia results are a little bit suspicious, using FEM based simulations could give better results.

Betatron oscillation is directly associated with field index (Equations 2.23 and 2.24). Since field index is assumed to be constant in these equations, radial and vertical betatron oscillations seem stable. However, in real life, frequency and amplitude of betatron oscillations can show alterations because of changing field index value.

5. CONCLUSION

In this thesis, the initial steps towards constructing Turkey's first MeV-energy cyclotron have been described. The design of the OZU Cyclotron has been drawn in both via Radia and AUTOCAD 3D software. Its main parts such as its iron yoke, electromagnets, and vacuum chamber have been constructed at the Özyeğin University Particle Accelerator Laboratory. Technical know how to built electromagnet double pancake coils at a modest budget and entirely with domestic resources have been established.

Magnetic field values in between the magnet poles have been measured for 5 A, 10 A, and 15 A at 4 cm intervals and 2 cm intervals respectively, producing a rough field map. Most of the $\frac{B}{I}$ values are piled up around 13×10^{-3} T/A in agreement with expectation. Measurement and Radia simulation have also been found to be compatible, furthermore, magnetic field measurement shows that an uniform magnetic field is created in the median plane.

An ion path simulation that utilizes 4th order Runge-Kutta method has been implemented in python. Sanity checks of this code has been performed using constant B value. A simulated magnetic field map obtained from Radia output has also been tested successfully.

Connection of a custom-built RF power amplifier to the system and the measurement of the flow parameters for cooling of the electromagnets have been left for future work. After their completion, attempts will be possible to obtain MeV-energy proton beam with Turkey's first domestically-built cyclotron.

REFERENCES

1. Morris, Jim, *1932 Cockroft and Walton, High Voltage Power Supply*, `http://www.scitechantiques.com/atomsmasher/`, accessed at May 2019.

2. University of Saskatchewan, *Van de Graaf Generator*, `https://openpress.usask.ca/physics155/chapter/3-3-calculations-of-electric-potential/`, accessed at May 2019.

3. Smith, Jeff, *Vacuum Chamber*, `http://departments.knox.edu/physicsdept/projects/Projects.htmCyclotron`, accessed at May 2019.

4. Barletta, A., William, *Cyclotrons: Old but Still New*, `http://uspas.fnal.gov/materials/12MSU/UTcyclotro- ns.pdf`, accessed at May 2019.

5. Winey, B. A., *A Low-Cost Van de Graaff Accelerator*, `https://www.houghton.edu/wp-content/uploads/2019/02/physics-thesis-winey.pdf`, accessed at May 2019.

6. Livingston, M., "The History of Cyclotron", *Proceedings of the 7th International Conference on Cyclotrons and their Applications, Zürich, Switzerland*, pp. 635–638, 1975.

7. *Ernest Lawrence and M. Stanley Livingston University of California, Berkeley*, `https://www.aps.org/programs/outreach/history/historicsites/lawrence livingston.cfm`, accessed at May 2019.

8. Green, C. H., "Technetium-99m production issues in the United Kingdom", *Journal of Medical Physics*, Vol. 37, 2012.

9. Guérin B, Tremblay S, Rodrigue S, Rousseau JA, Dumulon-Perreault V, Lecomte

R et al., "Cyclotron production of 99mTc: an approach to the medical isotope crisis.", *J Nucl Med.*, 2010.

10. Kerst, D. W., "The Acceleration of Electrons by Magnetic Induction", *Phys. Rev.*, Vol. 60, pp. 47–53, July 1941, `https://link.aps.org/doi/10.1103/PhysRev.60.47`.

11. Wilson, R. R., "Magnetic and Electrostatic Focusing in the Cyclotron", *Phys. Rev.*, Vol. 53, pp. 408–42, March 1938, `https://link.aps.org/doi/10.1103/PhysRev.53.408`.

12. Centre, P. M. T., *Magnetic Properties of Cast Irons*, `http://www.prizz.fi/sites/default/files/tiedostot/linkki2ID940.pdf`, accessed at May 2019.

13. Sylvia, M., "Focusing in the Houghton College Cyclotron", `https://www.houghton.edu/wp-content/uploads/2019/02/physics-thesis-sylvia-morrow-2015.pdf`, accessed at May 2019.

14. Koeth, Timothy, *Koeth Cyclotron Recent Ion Source*, `http://koethcyclotron.org/?page_id=507`, accessed at May 2019.

15. KONTHERM, *Kontherm KS-3518-010 Condenser Manual*, `http://www.kontherm.com/Assets/Documents/Standart-Kondenserler.pdf`, accessed at May 2019.

16. in collaboration with Klaus Halbach, R. F. H., *Poisson Superfish Software*, `https://laacg.lanl.gov/laacg/services/download_sf.phtml`, accessed at May 2019.

17. O. Chubar, J. C., P. Elleaume, *Radia Software*, `http://www.esrf.eu/Accelerators/Groups/InsertionDevices/Software/Radia`, accessed at May 2019.

18. PHYWE, *PHYWE Teslameter Operating Instructions*, `https://repository.curriculab.net/files/bedanl.pdf/13610.93/1361093e-.pdf`, accessed at May 2019.

19. "The Runge - Kutta Method of Numerically Solving Differential Equations", `The Runge - Kutta Method of Numerically Solving Differential Equations`, accessed at May 2019.

APPENDIX A: MAGNETIC FIELD AND ION PATH SIMULATIONS

A.1. The Magnetic Field Simulation Results

```
import matplotlib.pyplot as plt

import matplotlib.tri as tri

import numpy as np

import pandas as pd

from matplotlib.mlab import griddata

#matplotlib.use('GTK3Agg')

%matplotlib inline


df = pd.read_csv('mag_field_test_coarse.csv',

na_filter=False,

delimiter=",")

mask = (df.z==0)

x  = df[mask].x.values.flatten()

y  = df[mask].y.values.flatten()

Bx = df[mask].Bx.values.flatten()

By = df[mask].By.values.flatten()

Bz = df[mask].Bz.values.flatten()

z_min, z_max = -np.abs(Bz).max(), np.abs(Bz).max()


# ----------------------

# Interpolation on a grid

# ----------------------

# A contour plot of irregularly spaced data coordinates

# via interpolation on a grid.
```

```python
# Create grid values first.
xi = np.linspace(-230, 230, 93)
yi = np.linspace(-230, 230, 93)
# Perform linear interpolation of the data (x,y)
# on a grid defined by (xi,yi)
Bxi = griddata(x, y, Bx, xi, yi, interp='linear')
Byi = griddata(x, y, By, xi, yi, interp='linear')
Bzi = griddata(x, y, Bz, xi, yi, interp='linear')


fig1, ax1 = plt.subplots(nrows=1)
ax1.contour(xi, yi, Bxi, 50, linewidths=0.5, colors='k')
plt.xlabel('x (mm)')
plt.ylabel('y (mm)')
plt.title(r"Magnetic Field ($B_{x})$")
cntr1 = ax1.contourf(xi, yi, Bxi, 50, cmap="hot")
fig1.colorbar(cntr1, ax=ax1)
plt.gcf().set_size_inches(10, 8)
plt.savefig("Bx.pdf")
#plt.savefig("Bx.pdf")


fig2, ax2 = plt.subplots(nrows=1)
ax2.contour(xi, yi, Byi, 4, linewidths=0.5, colors='k')
plt.xlabel('x (mm)')
plt.ylabel('y (mm)')
plt.title(r"Magnetic Field ($B_{y})$")
cntr2 = ax2.contourf(xi, yi, Byi, 14, cmap="hot")
fig2.colorbar(cntr2, ax=ax2)
plt.gcf().set_size_inches(10, 8)
plt.savefig("By.pdf")+
```

```
        fig3, ax3 = plt.subplots(nrows=1)

        ax3.contour(xi, yi, Bzi, 20, linewidths=0.5, colors='k')

        plt.xlabel('x (mm)')

        plt.ylabel('y (mm)')

        plt.title(r"Magnetic Field ($B_{z})$")

        cntr3 = ax3.contourf(xi, yi, Bzi, 20, cmap="hot")

        fig3.colorbar(cntr3, ax=ax3)

        plt.gcf().set_size_inches(10, 8)

        plt.savefig("Bz.pdf")
\end{document}
```

A.2. Ion Path Simulation

```
        # -*- coding: utf-8 -*-

        from __future__ import print_function

        import numpy as np

        import matplotlib.pyplot as plt

        from mpl_toolkits.mplot3d import Axes3D

        import math as math

        import matplotlib.pyplot as plt

        import seaborn as sns

        import numpy as np

        %matplotlib qt

        from numba import vectorize, jit

        import time

        # import seaborn as sns

        from ipywidgets import interact, interactive, fixed,

        interact_manual

        import ipywidgets as widgets
```

```python
import pandas as pd
import itertools
import math
from termcolor import colored


def sign(x):
if x >= 0:
return 1
elif x==0:
return 0
else:
return -1


# sns.set()
beginning_time = time.time()


# SPEED OF LIGHT is 299792458 m/s
speed_of_light = 3.0E08


# number pi
pi = math.pi


number_of_points = 100


B_scale = 1.0


class Particle:
def __init__(self, pos, vel, mass, charge, energy=0):
self.pos = pos
self.vel = vel
self.mass = mass
```

```python
        self.charge = charge
        self.energy = energy



    # Print iterations progress
    def printProgressBar(iteration, total, prefix='',suffix='',
    decimals=1, length=100, fill='|'):
        """
        Call in a loop to create terminal progress bar
        @params:
        iteration   - Required  : current iteration (Int)
        total       - Required  : total iterations (Int)
        prefix      - Optional  : prefix string (Str)
        suffix      - Optional  : suffix string (Str)
        decimals    - Optional  : positive number of
        decimals in percent
        complete (Int)
        length      - Optional  : character length of bar (Int)
        fill        - Optional  : bar fill character (Str)
        """
        percent = ("{0:."+str(decimals)+"f}").format(100*(iteration/
        float(total)))
        filledLength = int(length*iteration // total)
        bar = fill*filledLength+'-'*(length - filledLength)
        print('\r%s |%s| %s%% %s' % (prefix, bar, percent,
        suffix), end='\r')
        # Print New Line on Complete
        if iteration == total:
        print()
```

```
# ## Set the Design Energy of The Cyclotron
# <br>As an example, let's set the desired energy of
the cyclotron as 2 MeV. Simulation will stop when this
energy is achieved. Also, we will set the separation of
the dees (in meter) and the voltage (in V) applied
between the plates. Then we will create our particle
object which is defined before in the code and name it
proton. <br>



# DESIRED ENERGY OF THE OUTCOMING IONS
desired_energy = 5E5
dee_sep = 2.0E-2
HV = 1.E4
# construct a particle named as "proton"
proton = Particle((0.0, -0.02, 0.0), [0.0,
1E-4*speed_of_light, 0.0], 1.67E-27, +1.60E-19, )


# ## Create the Magnetic and Electric Fields
# <br> Our dipole magnet will create a uniform
(hypothetically) magnetic field in the $z$-direction.
So we must create a vector as # <h3 align="center">
$\mathbf{B}=0\mathbf{i}+0\mathbf{j}+ B_z\mathbf{k}$ </h3>
## where $B_z$ is -1.1 Tesla


# MAGNETIC FIELD
df = pd.read_csv('mag_field_test.csv', na_filter=False,
delimiter=",")
x_mesh = np.arange(-230, 230, 10)
y_mesh = np.arange(-230, 230, 10)
z_mesh = np.arange(-20, 20, 5)
```

```python
@jit
def get_bounding_cube(point, x_mesh, y_mesh, z_mesh):
    x_bound_up = x_mesh.searchsorted(1E3*point[0])
    x_bound = [x_mesh[x_bound_up-1], x_mesh[x_bound_up]]
    y_bound_up = y_mesh.searchsorted(1E3*point[1])
    y_bound = [y_mesh[y_bound_up-1], y_mesh[y_bound_up]]
    z_bound_up = z_mesh.searchsorted(1E3*point[2])
    z_bound = [z_mesh[z_bound_up-1], z_mesh[z_bound_up]]

    bounding_cube = np.asarray(list(itertools.product(x_bound,
    y_bound, z_bound)))
    bounding_cube = bounding_cube.astype(float)
    return bounding_cube
@jit
def get_B_IDW(datasample, point, bounding_points, p=2,
metric=[1,1,1]):
    # get B values wrt Inverse Distance Weighting (IDW)
    B_x_idw = 0
    B_y_idw = 0
    B_z_idw = 0
    w_sum = 0
    for r in bounding_points:
        del_x = abs(1E3*point[0]-r[0])
        del_y = abs(1E3*point[1]-r[1])
        del_z = abs(1E3*point[2]-r[2])
        d = (metric[0]*del_x**2 + metric[1]*del_y**2 +
        metric[2]*del_z**2)**0.5

        if(d==0):
            d=1.
```

```
w = float(1./d**p)
mask = (datasample.x == r[0]) & (datasample.y == r[1]) &
(datasample.z == r[2])
#print(float(df[mask].Bz))
B_x_idw += w*float(df[mask].Bx)
B_y_idw += w*float(df[mask].By)
B_z_idw += w*float(df[mask].Bz)
w_sum += w
#print(B_idw/w_sum)
if(w_sum==0):
w_sum = 8.
#B = np.array([B_x_idw/w_sum, B_y_idw/w_sum, B_z_idw/w_sum])
B = np.array([0.0, 0.0, 0.68])
return np.multiply(B, B_scale)


# ELECTRIC FIELD
B_mean = B_scale*float(df[(abs(df.x) < 20) & (abs(df.y) < 20)
& (df.z == 0)].Bz.mean())
print(B_mean)
q, B, m = proton.charge, B_mean, proton.mass
w = q*(0.68)/m
phase = 0.0*(pi)


print("Gyro-Frequency = %2.2f rad/ns" % (1E-9*(q*B/m)))
print("Frequency = %2.2f MHz" % (1E-6*w/(2*pi)))


@jit
def e_field(t, phi=phase):
# if(np.cos(w*t+phi)<0):
#     E = [-(HV/dee_sep), 0.0, 0.0]
```

```
# else:
#     E = [(HV/dee_sep), 0.0, 0.0]
E = [(HV/dee_sep)*np.sin(w*t+phi), 0.0, 0.0]
return E


#  Returns the acceleration vector due to an electromagnetic
field ( from Lorentz force )
@jit
def em_acceleration(q_over_m, position, velocity,
magnetic_field, t):
#     calculated for a particle at position, with velocity


if abs(position[0]) >= dee_sep/2:
a = q_over_m*np.cross(velocity, magnetic_field)
else:
a = q_over_m*(np.array(e_field(t))+np.cross(velocity,
magnetic_field))


return a


v_i = np.linalg.norm(proton.vel)
expected_radius = v_i/((q*B/m))
print("Expected initial radius = %2.2f mm" %
(1E3*expected_radius))


expected_period = 2.0*pi/(B*(proton.charge/proton.mass))
print("Expected period = %2.2f ns" % (1E9*expected_period))


delta_t = expected_period/number_of_points
print("delta_t = %2.2f ns" % (1E9*delta_t))
# Count how many times the particle jumps from 1 D to
```

```
                the other
                jumps = 0
                jumps_max = int(desired_energy/(proton.charge*HV))


                # 4-th ORDER RUNGE-KUTTA METHOD
                @jit
                def rk4(particle, desired_energy, delta_t):
                q_over_m = q/m
                results = []


                #  Initial conditions
                i = 0
                p0 = np.array(particle.pos)
                v0 = np.array(particle.vel)
                t = 0
                energy = []


                # Distance traveled
                s = 0


                aux_index = 0


                while 0.5*particle.mass*(np.linalg.norm(v0)**2)/
                proton.charge <        (desired_energy):
                # for i in range(int(4E+4)):


                #if(i%100==0):
                #   print(i)
                if i > int(1E5):
                print(colored("Ion path is probably not stable!", "red"))
                break
```

```
bounding_cube = get_bounding_cube(p0,x_mesh,y_mesh,z_mesh)

B = get_B_IDW(df, p0, bounding_cube)

#print(p0, B)

#B = non_uniform_magnetic_field


p1 = p0

v1 = v0

a1 = delta_t*em_acceleration(q_over_m, p1, v1, B, t)

v1 = delta_t*v1


p2 = p0+(v1*0.5)

#bounding_cube = get_bounding_cube(p2,x_mesh,y_mesh,z_mesh)

#B = get_B_IDW(df, p2, bounding_cube)

v2 = v0+(a1*0.5)

a2 = delta_t*em_acceleration(q_over_m, p2, v2, B, t)

v2 = delta_t*v2


p3 = p0+(v2*0.5)

#bounding_cube = get_bounding_cube(p3,x_mesh,y_mesh,z_mesh)

#B = get_B_IDW(df, p3, bounding_cube)

v3 = v0+(a2*0.5)

a3 = delta_t*em_acceleration(q_over_m, p3, v3, B, t)

v3 = delta_t*v3


p4 = p0+v3

#bounding_cube = get_bounding_cube(p4,x_mesh,y_mesh,z_mesh)

#B = get_B_IDW(df, p4, bounding_cube)

v4 = v0+a3

a4 = delta_t*em_acceleration(q_over_m, p4, v4, B, t)

v4 = delta_t*v4
```

```
        dv = (a1+2.0*(a2+a3)+a4)
        v0 = v0+dv/6.0


        dp = (v1+2.0*(v2+v3)+v4)
        p0 = p0+dp/6.0


        results.append(p0.copy())
        t += delta_t
        i += 1
        s += np.linalg.norm(dp)/6
        energy.append(0.5*(particle.mass)*(np.linalg.norm(v0)**2)/
        proton.charge)


        if int(100*energy[-1]/desired_energy) > aux_index:
        # print(int(100*energy/desired_energy), aux_index)
        printProgressBar(int(100*energy[-1]/desired_energy), 100,
        prefix='Accelerating the Ion:',
        suffix='Complete', length=50)
        aux_index += 1


    print("Runge-Kutta method finished!")
    return s, results, energy


s, results, energy = rk4(proton, desired_energy, delta_t)
print("Distance traveled by the ion:%8.2f m" % s)


# PLOTTING
plt.style.use('seaborn')
# fig1 = plt.figure()
# ax[0 ,0] = fig1.add_subplot(1, 1, 1)
```

```python
# fig2 = plt.figure()
# ax[0, 1] = fig2.add_subplot(1, 1, 1)


# fig3 = plt.figure()
# ax[1, 0] = fig3.add_subplot(1, 1, 1)


# fig4 = plt.figure()
# ax[1, 1] = fig4.add_subplot(1, 1, 1)


# fig5 = plt.figure()
# ax[0, 2] = fig5.add_subplot(1, 1, 1)


width = 15
fig, axs = plt.subplots(2, 2, figsize=(width, width))


@jit
def part_plot(particle, max_iter, method, delta_t):
#  Mark the original position with a blue mark
x = []
y = []
z = []


x.append(particle.pos[0])
y.append(particle.pos[1])
z.append(particle.pos[2])
axs[0, 0].scatter(x, y, color='blue')


vz = []
v0 = np.linalg.norm(particle.vel)
#  use z array to save the velocity
```

```
        vz.append(v0)


    r = [np.linalg.norm(particle.pos[0:2])]


    energy[0:0] = [0.]


    print("initial position", x[0], y[0], vz[0])
    #   print " initial velocity", v0/speed_of_light,
    'the speed of light'
    print("initial velocity %1.4f the speed of light" %
    (v0/speed_of_light))


    # save the positions when in the spacing in a separate array
    #     so that w can change the color to red
    xc = []
    yc = []
    x = []
    y = []


    i = 0
    length = len(results)


    for p in results:


    vz.append(p[2])
    r.append(np.linalg.norm(p[0:2]))


    if p[0] >= dee_sep or p[0] <= -dee_sep:
    #inside the Dee's
    if len(xc):
    axs[0, 0].plot(xc, yc, color='red', linewidth=0.95)
```

```
        xc = []
        yc = []
        x.append(p[0])
        y.append(p[1])
        z.append(p[2])
    else:
    # inside the spacing
    if len(xc):
    axs[0, 0].plot(x, y, color='blue', linewidth=0.95)
    x = []
    y = []
    xc.append(p[0])
    yc.append(p[1])
    z.append(p[2])
    printProgressBar(i+1, length, prefix='Plotting Ion Path:',
    suffix='Complete', length=50)
    i += 1


    if len(xc):
    axs[0, 0].plot(xc, yc, color='red', linewidth=0.95)
    xc = []
    yc = []
    if len(x):
    axs[0, 0].plot(x, y, color='blue', linewidth=0.95)
    x = []
    y = []


    print("number of jumps between D's is", jumps)
    num_points = len(vz)
    #   print "final position",
    x[num_points-1],y[num_points-1],z[num_points-1]
```

```python
        print('number of points is', num_points, '*delta_t is total
        time = ', delta_t*num_points)


        axs[0, 0].set_title("Ion Position - Cyclotron")
        axs[0, 0].set_xlabel("Dimension-X (m)")
        axs[0, 0].set_ylabel("Dimension-Y (m)")


        t = np.linspace(0, len(z)*delta_t, len(vz))
        axs[0, 1].plot(np.multiply(r, 1E3), np.multiply(z, 1E3))


        axs[0, 1].set_xlabel("Radius (mm)")
        axs[0, 1].set_ylabel("z (mm)")


        axs[1, 0].plot(np.multiply(t, 1E6), np.multiply(z, 1E3))
        axs[1, 0].set_title("Time vs. z")
        axs[1, 0].set_xlabel("Time ("+chr(956)+"s)")
        axs[1, 0].set_ylabel("z (mm)")


        axs[1, 1].plot(np.multiply(t, 1E6), np.multiply(energy,1E-3))
        axs[1, 1].set_title("Time vs. Energy")
        axs[1, 1].set_xlabel("Time ("+chr(956)+"s)")
        axs[1, 1].set_ylabel("Energy (keV)")
        plt.savefig("energy.pdf")


        results_to_save = np.array(results).T
        x = np.insert(results_to_save[0], 0, 0.0)
        y = np.insert(results_to_save[1], 0, 0.0)
        z = np.insert(results_to_save[2], 0, 0.0)


        df = pd.DataFrame({"t" : t, "x" : x, "y" : y, "z" : z,
        "E" : energy})
```

```
        df.to_csv('cyclotron_path.csv', index=False)


        #print(len(t), len(x), len(y), len(z), len(energy))


        t1 = time.time()
        part_plot(proton, desired_energy, 'rk4', delta_t)
        print(time.time() - beginning_time)
        plt.tight_layout()
        plt.show()
        plt.savefig("plots.pdf")
```